



## Review Article

# Factors influencing the performance of solar air heater (SAH) having artificial coarseness: a review

Gaurav BHARADWAJ<sup>1,\*</sup>, Kamal SHARMA<sup>1</sup>, Kuwar MAUSAM<sup>1</sup>

<sup>1</sup>Department of Mechanical Engineering, GLA University, Mathura, India

## ARTICLE INFO

### Article history

Received: 6 December 2019

Accepted: 31 May 2020

### Key words:

Solar air heater; Nusselt number (Nu); Friction factor (f); Thermohydraulic performance variable ( $\eta$ )

## ABSTRACT

A review of studies focused on promoting the rate of heat transfer with the help of an optimum rise in friction factor, by offering a simulated irregularity to the interior surface of the absorber plate of SAH, is expressed. In this article an effort has been made to explore different coarseness configurations as used by number of researchers to boost the SAH heat transfer rate. Furthermore, different correlations developed by researchers for Nusselt number and friction factor are also presented. On the basis of these correlations, thermohydraulic performance variable was calculated and attributed for various coarseness configurations. Friction factor and Colburn factor of various coarseness configurations have also been compared and presented. This review focused on use of different coarseness configurations with different coarseness parameter and flow parameter is deeply discussed from which future researchers can easily identify that which coarseness is to be used for designing SAH duct for the better augmentation of heat transfer and friction factor. It also helps the researchers to determine the optimum value of coarseness parameter so that the SAH works efficiently and effectively.

**Cite this article as:** Bharadwaj G, Sharma K and Mausam K, Factors influencing the performance of solar air heater (SAH) having artificial coarseness: a review. J Ther Eng 2021;7(6):1556–1576.

## INTRODUCTION

Energy is an essential need to carry on with our everyday life at a cost of some significant things, for example, condition debasement by utilizing fossil powers. Utilization of non-renewable energy source is influencing the earth, as well as harming people's lives. The earth has settled amounts of these fossil powers held in it, which will be drained

following couple of years. Sustainable energy sources are becoming more important in the progressing days in this situation. Sustainable sources of power have broad truths that rely on use and area. Out of numerous sustainable power sources, solar energy has wide use in view of its enormous potential all over. Solar energy is a power source that is non – polluting, unreserved accessible and endless.

### \*Corresponding author.

\*E-mail address: [gauravmech2211@gmail.com](mailto:gauravmech2211@gmail.com),

[gaurav.bhardwaj@gla.ac.in](mailto:gaurav.bhardwaj@gla.ac.in)

*This paper was recommended for publication in revised form by  
Reginal Editor Ahmet Selim Dalkilic*



In any case, the capability for solar energy depends on the area of earth, climate, time, etc. Solar energy is easily absorbed by absorber into heat energy for heating purposes. SAH, in view of their natural straightforwardness are shabby and most generally utilized accumulation gadgets.

The fundamental utilizations of SAH are volume heating; flavoring of timber, drying of crops, etc. SAH involve an essential place among solar heating framework due to negligible utilization of resources [1].

The output of SAH in collation of water heating has been observed to be poor performer on account of their innately low heat exchange ability among the absorber plate and hot air crack in the channel. SAH effectiveness can be augmented by chiefly two main methods: 1. Reduction of heat losses, 2. augmenting the heat transfer rate. Due to its wide relevance, the second procedure is the most famous. Different systems are available to improve the applications - based heat exchange rate. Counterfeit coarseness make disturbance in the stream of air upon the warm surface and try to terminate the warm boundary layer. Different researchers have strived to propose a coarseness component that could improve convective heat transfer rate with least increment in friction drop [2–4]. Many researchers have also worked over the numerical analysis of turbulent forced convection flow in solar air channel with different coarse baffles. They also worked to enhance the heat transfer of the solar air channel using different baffle configuration [5,6,7–14,15–24].

In this article, an endeavor has been made to summarize the different coarseness configuration used in SAH. Section 2 of the review paper deals with the theory behind the artificial coarseness and what are the different coarseness parameter which is to be included while developing the correlations using various configurations. Section 3 deals with the performance evaluation of conventional SAH. This section gives the concept and formulae which is to be used for evaluating thermohydraulic performance of SAH. Section 4 deals with the different coarseness parameter and their consequences on heat transfer and friction factor. Section 5 deals with the detailed literature on the utilization of different configuration used by various researchers for various coarseness and flow parameters. This section also shows the impact of coarseness parameter and flow parameters on the augmentation of heat transfer and friction factor used by various researchers. Section 6 deals with evaluation of thermohydraulic parameter for various coarseness configurations and identifying which coarseness provides the better augmentation in heat transfer. Section 7 deals with evaluation of colburn factor and friction factor for various coarseness configurations and identifying which coarseness provides the better augmentation in friction factor.

One of the most effective techniques for the intensification in the heat transfer is to provide the random coarseness

on the heat exchange surface. Surface coarseness is the first promising technique to be taken into account for the augmentation of forced convection heat transfer. To achieve better heat transfer coefficient, the stream close to heat transfer surface ought to be turbulent. On the other hand, energy for generating these disturbances has to derive from the fan or blower and the exorbitant disturbance has consumed exorbitant power to make the air stream through the channel.

Henceforth, it's essential that the disturbance must occurs in the area of heat transfer surface i.e. hydrodynamic sub layer just where the heat transfer occurs and the stream ought not to be unreasonably aggravated in order to keep away from exorbitant friction drops. This should be possible by maintaining the height of the coarseness component to be little in contrast to channel size [25].

## THERMAL AND STREAM ATTRIBUTES OF FLUID OVER ROUGH SURFACE

Due to the tangled essence of the stream, it is very complex to derive an analytical stream model for the stream over a rough surface comprising turbulence. Subsequently, early investigations begin with that of Nikuradse. He tried to create speed and thermal flow pattern over rough surfaces [25]. The various relations proposed by Nikuradse are as follows:

### Smooth Stream Regime

$$u^+ = y^+ \text{ For hydrodynamic sub layer, } y^+ \leq 5 \quad (1)$$

$$u^+ = 5 \ln y^+ + 3.5 \text{ For buffer layer, } 5 \leq y^+ \leq 30 \quad (2)$$

$$u^+ = 2.5 \ln y^+ + 5.5 \text{ For turbulent layer, } y^+ > 30 \quad (3)$$

### Stream over Rough Surface

A detailed study over rough surface demonstrated that velocity profile in the turbulent stream regime powerfully depends on the coarseness height as well as the Reynolds number (Re). A new variable Coarseness Reynolds number ( $e^+$ ) was derived as a outcome of coarseness height and stream Re as

$$e^+ = \frac{e}{D} \sqrt{\frac{f}{2}} Re \quad (4)$$

$$R(e^+) = \sqrt{\frac{2}{f}} + 2.5 \ln \left( \frac{2e}{D} \right) + 3.75 \quad (5)$$

A similar relation was developed by Dippery and Sabersky [26] to find out the heat transfer for circular rough tubes which is written as,

$$G(e^+) = \left[ \frac{f}{2St} - 1 \right] \sqrt{\frac{f}{2}} + R(e^+) \quad (6)$$

Gee and Web [27] developed correlations for friction coarseness and heat transfer as the function of coarseness variable was as follows,

$$R(e^+) = \left[ \sqrt{\frac{2}{f}} - 2.5 \ln \left( \frac{2e}{D} \right) + 3.75 \right] \left( \frac{\alpha_a}{50} \right)^{0.16} \quad (7)$$

$$G(e^+) = \left[ \frac{f/2 \cdot St - 1}{\sqrt{f/2}} + R(e^+) \right] \left( \frac{\alpha_a}{50} \right)^J \quad (8)$$

Where,  $J = 0.37$  for  $\alpha_a < 50^\circ$  and  $J = -0.16$  for  $\alpha_a > 50^\circ$

Experimental information gathered on different configurations of rib roughened surfaces was applied for the creation of relationship of the form,

$$R = R(e^+, p/e, \alpha, e/D, \text{channel shape, rib shape}) \quad (9)$$

$$G = G(e^+, p/e, \alpha, e/D, \text{channel shape, rib shape}) \quad (10)$$

It was consequently understood that the empirical correlations might be more correct for model and analyze accordingly. These developed correlations are the outcome of Re, Dimensionless coarseness pitch ( $p/e$ ), Dimensionless coarseness height ( $e/D_h$ ), angle of attack ( $\alpha$ ), aspect ratio of channel ( $W/H$ ) and the geometry of the rib.

## PERFORMANCE EVALUATION OF CONVENTIONAL SAH

For the proficient layout of such a model, it is important to consider the thermal and thermohydraulic performance. Thermal performance cope with the effective heat transfer through the SAH absorber plate and thermohydraulic performance deals with the pressure drop ( $\Delta P$ ) in the channel [28]. A traditional SAH used for the concise evaluation of thermal performance and thermohydraulic performance is shown in Fig. 1.

### Thermal Performance

Thermal performance tells about how efficiently the absorber plate can transfer heat to the working fluid i.e. air.

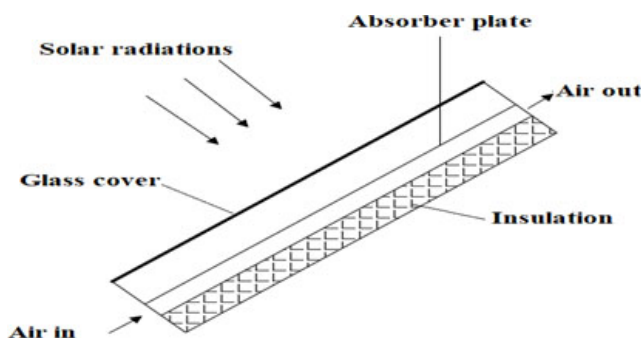


Figure 1. Traditional SAH.

Hottel–Whillier–Bliss equation is utilized to find out tangible heat increase to air in SAH channel which was reported by Duffie and Beckman [29].

$$q_u = F_R [I(\tau\alpha)_e - U_L(T_i - T_a)] \quad (11)$$

The equation for the thermal efficiency can be given as,

$$q_u = F_R \left[ I(\tau\alpha)_e - U_L \left( \frac{T_i - T_o}{I} \right) \right] \quad (12)$$

### Hydraulic Performance

Hydraulic performance of a SAH pact with  $\Delta P$  in the channel.  $\Delta P$  represents energy utilization by fan to impel air through the channel.  $\Delta P$  can be spoken to in non-dimensional shape by utilizing the accompanying correlation of friction factor ( $f$ ), revealed by Frank and Mark [30].

$$f = \frac{(\Delta P) D_h}{2\rho L V^2} \quad (13)$$

A SAH is said to be effective if maximum heat transfer occur at minimum power consumption. Thermohydraulic performance in addition to the thermal performance helps in the selection of SAH design. The concept of thermohydraulic performance variable was given by Lewis [31] which is as follows,

$$\eta = \frac{(Nu / Nu_s)}{(f / f_s)^{1/3}} \quad (14)$$

## IMPACT OF COARSENESS VARIABLES ON STREAM PATTERN

In this segment of the article, the consequence of different coarseness constraints on stream pattern is discussed.

### Consequence of Rib

The essential impact created by the occurrence of a rib on the stream is the segregation of the stream, along with each side of the rib. The segregation of the stream thus produced is responsible for the turbulence generation and thereafter also augments the heat transfer rate and friction losses as well.

### Consequence of $e/D_h$

The consequence of  $e/D_h$  on the stream pattern was revealed by Prasad and Saini [32]. Reattachment points and segregation of stream takes place in the domain of the ribs. Reattachment points are formed for the sufficiently low value of  $e/D_h$  and the greater value of the Dimensionless coarseness pitch is not reattached as in Fig. 2. Each pitch arrangement offers the most favorable rib height span. Though extensive large rib disturbs the stream prompting high pumping power.

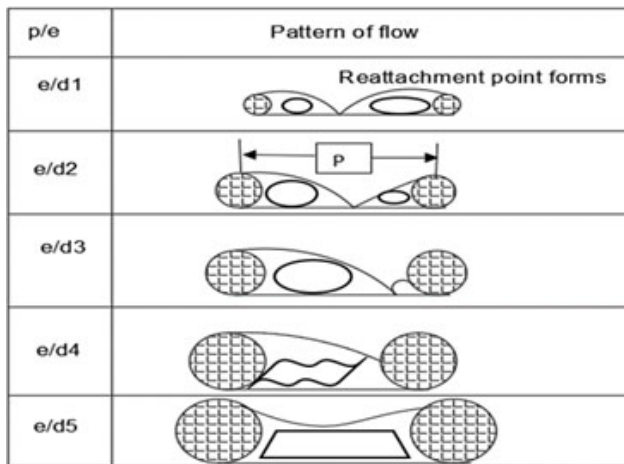


Figure 2. Effect of coarseness relative height.

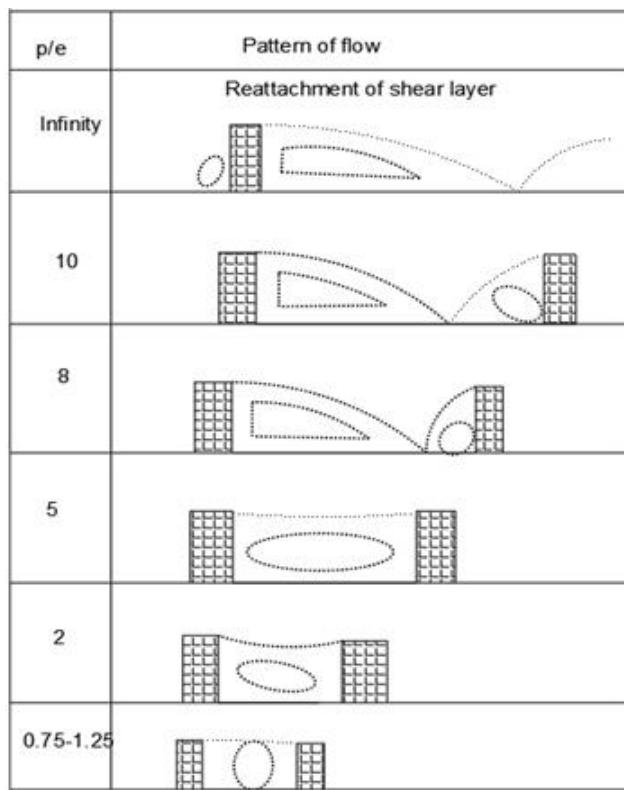


Figure 3. Effect of relative coarseness height.

### Consequence of P/E

The consequence of p/e on the stream pattern was also revealed by Prasad and Saini [32] which is shown in Fig. 3. They found that there is no reattachment of the hydrodynamic sub layer at p/e less than 8 due to segregation of stream near the rib. The p/e value suggested by them is between 8 and 10. After p/e of 10, value of reattachment point get reduced owing to reduce in number of ribs.

Therefore, maximal heat transfer obtains in between p/e from 8 to 10.

### Consequence of Inclination of Rib ( $\alpha$ )

The consequence of inclination of rib has been revealed by M.E. Taslim [33]. The major span wise variation in the heat transfer coefficient is responsible for the counter secondary stream generated by rib inclination. He has shown that the secondary stream generated joins the primary stream abruptly, i.e. air moving from the rib's trailing verge to the rib's lagging verge. Augmentation in heat transfer occurs when the secondary stream brought the cooler channel into contact with the rib's leading edge while the lagging heat transfer is comparatively low.

### Consequence of V-Shaping of Rib

The consequence of V-shaping of rib has been revealed by M.E. Taslim [33]. Breaking of a long-tilted rib into V-shape helps to generate two secondary stream patterns, which in turn improves the overall heat transfer rate in contrast to the long-tilted rib.

### Consequence of Gap in Ribs

The consequence of gap in ribs has been revealed by Aharwal et al. [34]. If the gap is provided in continuous inclined rib, the secondary stream across the rib merges the main stream to increase its velocity, which facilitates the retarded boundary layer stream across the surface, thereby augmenting the heat transfer rate over the gap width region back to the rib.

### Consequence of Rib Cross-Section

The rib cross-section also relies on heat and stream attributes as different rib cross segments make distinctive disturbance level in the stream. Larger amount of disturbance level and stream mixing prompts higher heat transfer. Round ribs give the low heat transfer rate because of low level of turbulence and low value of heat transfer area. Round ribs additionally show low  $\Delta P$  because of low level of disturbance in the stream because of its continual surface [35].

## UTILIZATION OF VARIOUS COARSENESS GEOMETRIES IN SAH

Many researchers probed the consequence of artificial coarseness on the heat transfer rate and the friction losses. Furthermore, different correlations developed for Nu and f as the function of the operating and coarseness variables. Consequences of different configurations on heat transfer and stream attributes are discussed in this segment of the paper.

### Transverse Ribs

The ribs are affixed to the inner face of the absorber plate perpendicular to the stream of the air. Number of the

researchers probed the consequence of transverse rib on the heat transfer and the stream attributes as given below.

#### Continuous transverse ribs

Prasad and Saini [32][36] have been examined the consequence of  $e/D_h$ ,  $p/e$  and  $Re$  on heat transfer and friction factor. The span of various coarseness variable and stream variables taken into consideration for the experimentation were  $Re$  from 5000 to 50000,  $e/D_h$  from 0.02 to 0.033 and  $p/e$  from 10 to 20. They found that maximal heat transfer occurs close to the reattachment point. When the coarseness height is higher than the hydrodynamic sublayer the goal of optimal thermohydraulic performance is accomplished. Maximal augmentation in the heat transfer and friction factor was observed to be 2.38 and 4.25 folds that of smooth channel. They found that maximal heat transfer augmentation occurs at  $e/D_h$  of 0.033 and  $p/e$  of 10. The configuration used by Prasad and Saini [36] is given in Fig. 4.

Gupta et al. [37] have been examined the consequence of transverse rib coarseness on heat transfer and stream attributes in transitionally rough stream region ( $5 < e^+ < 70$ ). The span of various coarseness variable and stream variables taken into consideration for the experimentation were  $Re$  span of 3000–18000 for a  $W/H$  of 6.8–11.5,  $e/D_h$  of 0.018–0.052,  $p/e$  of 10,  $e^+$  between 5–70. They observed that the Stanton number augments initially with the  $Re$  up to approximately 12000 where it reaches the maximal value and after it there is a insignificant fall in the Stanton number. They have developed correlations for transitionally rough stream region in terms of coarseness variable and stream variables.

Verma and Prasad [38] have been examined the consequence of continuous transverse rib coarseness on heat transfer. The span of different coarseness variable and stream variables taken into consideration for the experimentation were  $Re$  from 5000 to 20000,  $p/e$  from 10 to 40,  $e/D_h$  0.01 to 0.03 and coarseness Reynolds number 8 to 42. They found that best value of thermohydraulic performance is near to 71% for  $e^+$  of 24.

#### Transverse broken ribs

Sahu and Bhagoria [39] have been examined the consequence of transverse broken ribs on the heat transfer coefficient. The span of various coarseness variable and stream variables taken into consideration for the experimentation

were coarseness pitch spans from 10–30 mm, rib height 1.5 mm,  $Re$  spans from 3000–12,000. They found that heat transfer has the maximal value at the coarseness pitch 20 mm and goes on decreasing with increment in  $p/e$ . For the given stream condition, it was observed that maximal thermal effectiveness of roughened SAH is of the order of 51–83.5%. Coarseness on the absorber plate augment the heat transfer coefficient 1.25–1.4 times as that of the smooth channel. Configuration used by them is given in Fig. 5.

#### Inclined Ribs

Ribs are affixed to the undersurface of the absorber plate of the SAH at the inclination w.r.t. stream of air. Many researchers discuss the consequences of inclination of ribs on the heat transfer and stream attributes which are explained under this section.

#### Continuous inclined ribs

Gupta et al. [40] have been examined the consequence of continuous inclined ribs on the heat transfer rate and friction factor. The span of various coarseness variable and stream variables taken into consideration for the experimentation were  $e/D_h$  from 0.023 to 0.5, inclination of rib  $60^\circ$  w.r.t stream direction and  $Re$  from 3000 to 18000. They found that thermohydraulic performance also increases with the augmentation in solar intensity. For a roughened SAH, maximal augmentation in heat transfer and friction factor was observed to be 1.8 and 2.7 folds respectively for  $\alpha$  of  $60^\circ$ . Maximum thermohydraulic performance was observed for  $e/D_h$  of 0.023 and at  $Re$  of 14000.

#### Inclined ribs with gap

Aharwal et al. [34] have been examined the consequence of inclined ribs with gap on the heat transfer rate and stream attributes. They have varied the span of gap width from 0.5 to 2 and gap position from 0.1667 to 0.667 respectively to see their effect on heat transfer for the fixed value of  $p/e$  of 10,  $e/D_h$  of 0.0377, and  $\alpha$  of  $60^\circ$ . The maximal augmentation in  $Nu$  and friction factor was found to be 2.59 and 2.87 folds, respectively. The thermohydraulic performance variable was reported to be the maximal for the  $d/W$  of 1.0 and  $g/e$  of 0.25.

Later on, Aharwal et al. [41] also seen the effect varying  $e/D_h$ ,  $p/e$  and angle of attack of inclined ribs with gap on

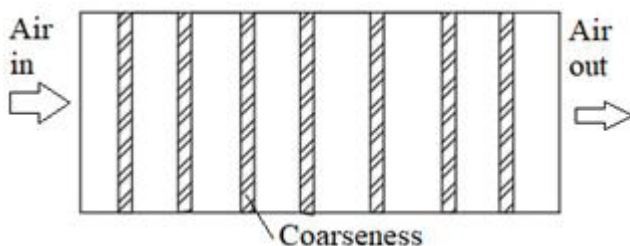


Figure 4. Transverse continuous ribs.

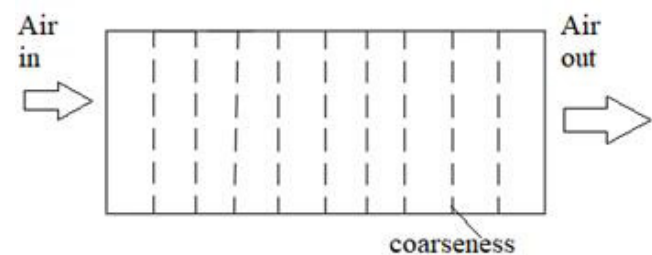


Figure 5. Transverse broken ribs.

the heat transfer and stream attributes. They have varied the span of  $p/e$  from 4 to 10,  $e/D_h$  from 0.018 to 0.0377, and angle of attack ( $\alpha$ ) of  $30^\circ$  to  $90^\circ$ . The maximal augmentation in Nu and friction factor was recorded to be 2.83 and 3.6 folds, respectively. The maximal augmentation in Nu and friction factor was recorded at  $g/e$  of 0.25 for  $d/W$  of 1.0,  $p/e$  of 8.0,  $\alpha$  of  $60^\circ$  and  $e/D_h$  of 0.037. As a function of coarseness variables and stream variables, correlation for Nu and friction factor was derived. Configuration of ribs used by them is shown in Fig. 6.

**Alphabetic Arrangement of Ribs**

The effect of ribs arranged in alphabetic shape to the undersurface of the absorber plate is discussed below.

**Continuous single v shaped ribs**

Momin et al. [42] have investigated the consequence of continuous V-shaped ribs on heat transfer and fluid stream attributes. The various variables taken into consideration during the investigation were Re from 2500 to 18000,  $e/D_h$  from 0.02 to 0.034 and  $\alpha$  from  $30^\circ$  to  $90^\circ$  for a fixed  $p/e$  of 10. The maximal augmentation of Nu and friction factor was reported to be 2.30 and 2.83 folds, respectively for  $\alpha$  of  $60^\circ$ . They also compared their result with the continuous inclined ribs for same angle of attack and came to conclude that the Nusselt number gets enhanced by 1.14 times w.r.t. inclined ribs. As a function of coarseness and stream variables, correlation for Nu and friction factor were derived. Configuration used by them is represented in Fig. 7.

**Multiple v shaped ribs**

Hans et al. [43] have discussed the consequence of continuous multiple V shape ribs on heat transfer and stream attributes. The span of variables taken into consideration were Re from 2000 to 20000,  $e/D_h$  from 0.019 to 0.043,  $p/e$  from 6 to

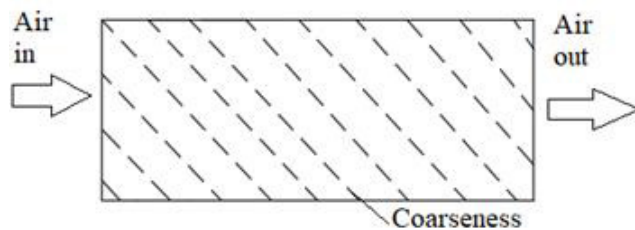


Figure 6. Inclined broken ribs.

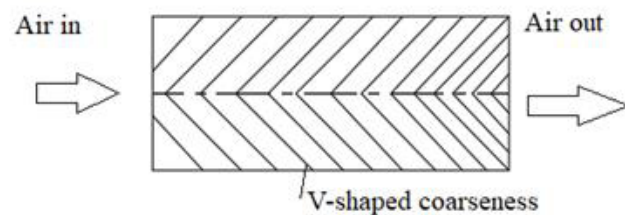


Figure 7. V-shaped coarseness.

12, angle of attack from  $30^\circ$  to  $75^\circ$  and  $W/w$  from 1 to 10. The maximal heat transfer and friction factor was recorded at  $W/w$  of 6 and 10 respectively corresponding to a  $60^\circ$  and  $p/e$  10. They found that augmentation of Nu and friction factor were 6 and 5 folds, respectively. As a function of coarseness variables and stream variables, correlations for Nu and friction factor were derived. Configuration used by them is shown in Fig. 11.

**W shaped ribs**

Lanjewar et al. [44] done an experiment to study the thermo-hydraulic performance of SAH using W-shaped ribs on absorber plate. W-shaped ribs have been investigated under downstream and upstream condition. The various variables taken into consideration were  $e/D_h$  of 0.03375,  $p/e$  of 10 and Re from 2300 to 14000. They found that thermo-hydraulic performance ratio of roughened absorber plate is in the span of 1.46–1.95 for W-down and 1.21–1.73 for W-up ribs.

Later on, Lanjewar et al. [42] they found the effect of  $e/D_h$  from 0.018 to 0.03375,  $\alpha$  from  $30^\circ$  to  $75^\circ$ , Re from 2300 to 14000 respectively at fixed  $p/e$  of 10 using W shaped ribs. They found that augmentation of Nu and friction factor was 2.36 and 2.01 folds, respectively. As a function of coarseness variables and stream variables, correlations for Nu and friction factor were derived. Configuration used by them is shown in Fig. 9.

**S shaped ribs**

Kumar et al. [45] have been examined the consequence of S shape ribs on heat transfer and friction factor. The

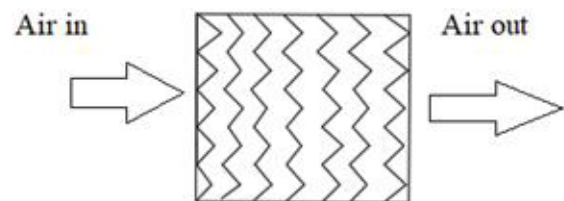


Figure 8. Multiple V shaped ribs.

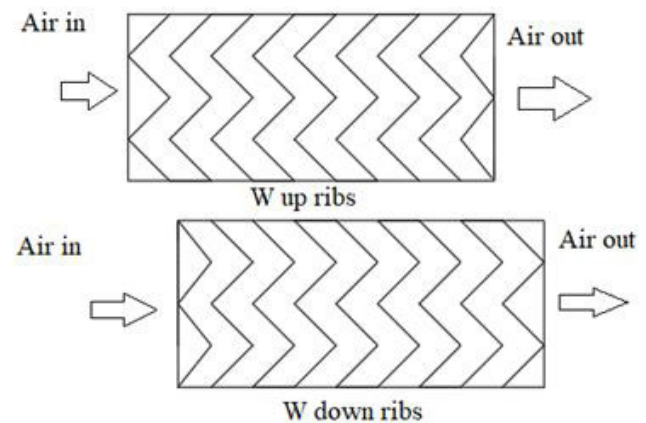


Figure 9. W shaped ribs.

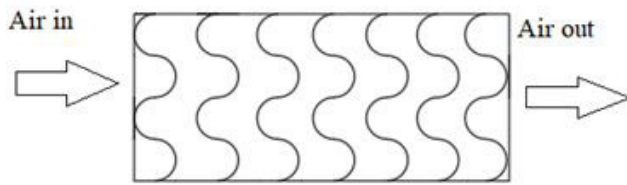


Figure 10. S-shaped ribs.

various variables taken into consideration were  $Re$  from 2400 to 20000,  $p/e$  from 4 to 16,  $e/D_h$  from 0.022 to 0.054, from  $30^\circ$  to  $75^\circ$ ,  $W/w$  from 1 to 4. They observed that maximal augmentation in  $Nu$  and friction factor was obtained at  $W/w$  of 3,  $p/e$  of 8,  $\alpha$  of  $60^\circ$  and  $e/D_h$  of 0.043. The maximal augmentation in  $Nu$  and friction factor was recorded to be 4.64 and 2.71 folds, respectively. As a function of coarseness variables and stream variables, correlations for  $Nu$  and friction factor were derived. Configuration used by them is shown in Fig. 10.

#### V shaped ribs with single gap

Singh et al. [46] have been examined the consequence of V-down rib having gap on thermohydraulic performance of roughened rectangular channels roughened. The various variables taken into consideration were  $Re$  from 3000 to 15,000,  $\alpha$  from  $30^\circ$  to  $75^\circ$  for the fixed  $e/D_h$  of 0.043 and  $p/e$  of 8. They observed that maximal value of thermohydraulic performance variable was 2.06 w.r.t  $\alpha$   $60^\circ$ . Later on, Singh et al. [47] determined the consequence on heat transfer and friction factor for various coarseness variables and stream variables. They varied the  $Re$  from 3000 to 15000,  $d/w$  of 0.5 to 2,  $g/e$  from 0.2 to 0.8,  $p/e$  from 4 to 12, angle of attack from  $30^\circ$  to  $75^\circ$  and  $e/D_h$  from 0.015 to 0.043. The maximal augmentation in  $Nu$  and friction factor was observed to be 3.04 and 3.11 folds respectively. They also found that maximal value of  $Nu$  and friction factor determined at  $g/e$  of 0.65,  $d/w$  of 1.0, and  $p/e$  of 8.0,  $\alpha$  of  $60^\circ$  and  $e/D_h$  of 0.043. As a function of coarseness variables and stream variables, correlations for  $Nu$  and friction factor were derived.

Futher, Singh et al. [48] evaluated thermal performance of SAH roughened with V Shape ribs with gap. They found that the best value of thermal performance occurred at  $g/e$  of 0.65,  $d/w$  of 1.0,  $p/e$  of 8.0,  $\alpha$  of  $60^\circ$  and  $e/D_h$  of 0.043.

#### V shape ribs with symmetrical multiple gap

Maithani and Saini [49] have been examined the consequence of V shape ribs having symmetrical multiple gap used as coarseness element on the absorber plate for augmentation of heat transfer in SAH. The span of stream variable and coarseness variables taken into consideration were  $Re$  from 4000 to 18,000, Number of gaps from 1 to 5,  $g/e$  from 1 to 5,  $p/e$  from 6 to 12, angle of attack from  $30^\circ$  to  $75^\circ$  and  $e/D_h$  of 0.043. The maximal augmentation in  $Nu$  and friction factor

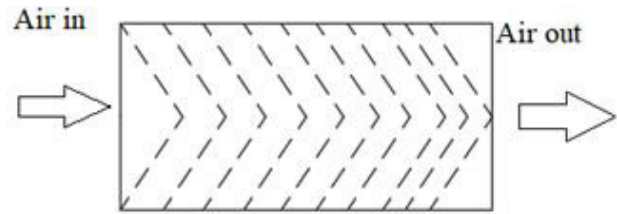


Figure 11. V shaped ribs with symmetrical gap.

was recorded to be 3.6 and 3.67 folds respectively. They also found that maximal value of  $Nu$  and friction factor occurred at  $g/e$  of 4.0,  $p/e$  of 10,  $\alpha$  of  $60^\circ$  and gap number 4. As a function of coarseness variables and stream variables, correlations for  $Nu$  and friction factor were derived. Configuration used by them is shown in Fig. 11.

#### Multiple v shape ribs with gap

Kumar et al. [50] have been examined the consequence of multiple V shape ribs having gap used as coarseness element over the absorber plate for augmentation of heat transfer in SAH. The span of stream variable and coarseness variables taken into consideration were  $Re$  from 2000 to 20,000,  $Gd/Lv$  from 0.24 to 0.80,  $g/e$  from 0.5 to 1.5 whereas  $W/w$ ,  $e/D_h$ ,  $p/e$  and  $\alpha$  were fixed at 6, 0.043, 10 and  $60^\circ$  respectively. The maximal augmentation in  $Nu$  and friction factor was found to be 6.32 and 6.12 folds respectively. The thermo-hydraulic performance variable was recorded to be best for the  $Gd/Lv$  of 0.69 and  $g/e$  of 1.0.

Later on, Kumar et al. [51] discussed the effect of varying  $e/D_h$ ,  $p/e$  and  $\alpha$  which were kept constant in their previous investigation. The various variables taken into consideration were  $Re$  from 2000 to 20,000,  $Gd/Lv$  from 0.24 to 0.80,  $g/e$  from 0.5 to 1.5 whereas  $W/w$  from 1 to 10,  $e/D_h$  from 0.022 to 0.043,  $p/e$  from 6 to 12 and  $\alpha$  from  $30^\circ$  to  $75^\circ$ . The maximal enhancement in  $Nu$  and friction factor was recorded to be respectively 6.74 and 6.37 folds. The coarseness variables at which maximal augmentation in  $Nu$  and friction factor were found at  $Gd/Lv$  of 0.69,  $g/e$  of 1.0,  $e/D_h$  of 0.043,  $p/e$  of 8,  $W/w$  of 6 and  $\alpha$   $60^\circ$ . As a function of coarseness variables and stream variables, correlations for  $Nu$  and friction factor were derived.

#### Discrete w shape ribs

Kumar et al. [52] have been examined the consequence of discrete W shape ribs used as coarseness element over the absorber plate for augmentation of heat transfer in SAH. The various stream variable and coarseness variables taken into consideration were  $Re$  from 3000 to 15,000,  $e/D_h$  from 0.0168 to 0.0338,  $p/e$  of 10 and  $\alpha$  from  $30^\circ$  to  $75^\circ$ . The maximal augmentation in  $Nu$  and friction factor was reported to be respectively 2.16- and 2.75-folds w.r.t  $\alpha$  of  $60^\circ$ . As a function of coarseness variables and stream variables, correlations for  $Nu$  and friction factor were derived. Configuration used by them is shown in Fig. 12.

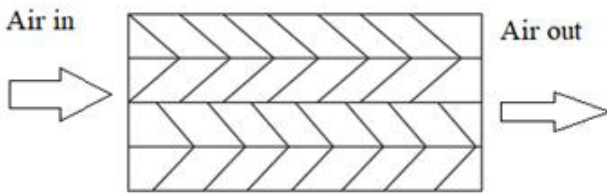


Figure 12. Discrete w-shaped ribs.

**Arc Shape Ribs**

Many investigators have seen the effect of ribs arranged in arc shape to the undersurface of the absorber plate for the augmentation of heat transfer and friction factor in SAH which are stated below.

**Single arc shape ribs**

Saini and Saini [53] have been examined the consequence of continuous arc shape ribs used as coarseness element over the absorber plate for augmentation of heat transfer in SAH. The various stream variable and coarseness variables taken into consideration were Re from 2000 to 17,000,  $e/D_h$  from 0.0213 to 0.0422,  $p/e$  of 10 and  $\alpha$  from 30° to 60°. The maximal augmentation in Nu and friction factor was reported to be respectively 3.80 and 1.75 folds w.r.t  $\alpha$  of 60°. As a function of coarseness variables and stream variables, correlations for Nu and friction factor were derived.

Sahu and Prasad [54] evaluated the exergetic performance of SAH with continuous arc shape ribs affixed to the undersurface of the absorber plate. The various stream variable and coarseness variables taken into consideration were similar to Saini and Saini. They found that maximum exergetic efficiency was 56% for the roughened SAH and the optimum value of  $e/D_h$ ,  $p/e$  and  $\alpha$  was 0.0422, 10 and 60° respectively. Configuration used by them is shown in Fig. 13.

**Multiple arc shape ribs**

Singh et al. [55] have been examined the consequence of multiple arc shapes ribs attached to the undersurface of the absorber plate for the augmentation of heat transfer and friction factor in SAH. The various variables taken into account during experimentation were Re from 2200 to 22,000,  $e/D_h$  from 0.018 to 0.045,  $\alpha$  from 30° to 75°,  $W/w$  from 1 to 7 and  $p/e$  from 4 to 16. They found that maximal augmentation obtained in Nu and friction factor was 5.07 and 3.71 respectively. The maximal augmentation for Nu was obtained at

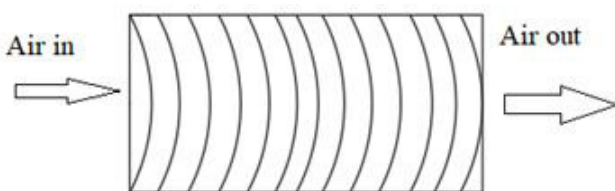


Figure 13. Single arc shaped ribs.

Re value of 22,300,  $W/w$  of 5,  $e/D_h$  of 0.045,  $p/e$  of 8 and a 60° while maximal friction factor was obtained at Re value of 22,300,  $W/w$  of 7,  $e/D_h$  of 0.045,  $p/e$  of 8 and a 60°. As a function of coarseness variables and stream variables, correlations for Nu and friction factor were derived.

Further, Singh et al. [56] determined the thermohydraulic performance of the SAH having multiple arc shape ribs. They found that maximum thermohydraulic performance was 3.4 corresponding to Re of 22300,  $e/D_h$  of 0.045,  $W/w$  of 5,  $p/e$  of 8 and a 60°. Configuration used by them is shown in Fig. 14.

**Multiple arc shape ribs with gap**

Pandey et al. [57] have been examined the consequence of multiple arc shape with gap attached to the undersurface of the absorber plate for the augmentation of heat transfer and friction factor in rectangular channel. The different stream variable and coarseness variables taken into account for experimentation were Re from 2100 to 21000,  $e/D$  from 0.016 to 0.044,  $p/e$  from 4 to 16,  $\alpha$  from 30° to 75°,  $W/w$  from 1 to 7,  $d/x$  from 0.25 to 0.85 and  $g/e$  from 0.5 to 2.0. The maximal augmentation in Nu and friction factor was found to be 5.85 and 4.96 times respectively. The maximal augmentation for Nu was found at Re 21000,  $W/w$  5,  $d/x$  0.65,  $g/e$  1,  $e/D_h$  0.044,  $p/e$  8 and  $\alpha$  60°. As a function of coarseness variables and stream variables, correlations for Nu and friction factor were derived. Configuration used by them is shown in Fig. 15.

Further, Pandey and Bajpai [58] evaluated the thermal efficiency for SAH having multiple arc shape ribs. They found that the maximal thermal efficiency was obtained at  $e/D_h$  0.045,  $p/e$  8,  $\alpha$  60°,  $g/e$  1,  $W/w$  5 and  $d/x$  0.65.

**Dimple Shape Ribs**

**Transverse dimple arrangement**

Saini and Verma [59] have been examined the consequence of dimple-shape coarseness and stream variables on heat transfer and friction factor in SAH. The various stream variable and coarseness variable taken into account for the



Figure 14. Multiple arc shaped ribs.

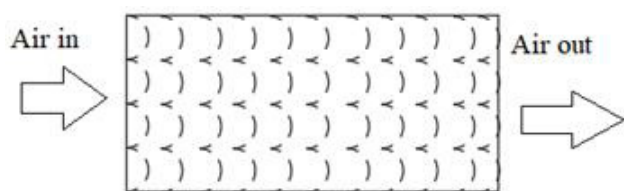


Figure 15. Multiple arc shape ribs with gaps.

experiment were  $Re$  from 2000 to 12,000,  $e/D_h$  from 0.018 to 0.037 and  $p/e$  from 8 to 12. They reported that the maximal value of  $Nu$  was obtained at  $e/D_h$  of 0.0379 and  $p/e$  of 10 while minimal value of friction factor was at  $e/D_h$  of 0.0289 and  $p/e$  of 10. As a function of coarseness variables and stream variables, correlations for  $Nu$  and friction factor were derived. Configuration used by them is shown in Fig. 16.

#### Arc shape dimple arrangement

Sethi et al. [60][61] have been examined the consequence of dimple-shape coarseness arranged in arc fashion and operating variables on heat  $e/D_h$  transfer and friction factor in SAH. The various stream variable and coarseness variable taken into account for the experiment were  $p/e$  from 10 to 20,  $e/D_h$  from 0.021 to 0.036,  $\alpha$  from  $45^\circ$  to  $75^\circ$ , and  $Re$  from 3600 to 18 000. They reported that the maximal value of  $Nu$  was obtained at  $p/e$  of 10,  $\alpha$   $60^\circ$  and  $e/D_h$  of 0.036. They also evaluated the thermohydraulic performance variable that lies in between 1.18 to 1.887. As a function of coarseness variables and stream variables, correlations for  $Nu$  and friction factor were derived. Configuration used by them is shown in Fig. 17.

#### Multiple v dimple arrangement

Kumar et al. [62] have been examined the consequence of multiple V-dimple-shape coarseness and stream variables on heat transfer and friction factor in SAH. The various stream variable and coarseness variable taken into account for the experiment were  $Re$  from 5000 to 17000,  $W_c/W_d$  from 1 to 6,  $e_d/d_d$  from 0.50 to 2.0, and from 8.0 to 11.0, and  $e_d/D_h$  of 0.037 and  $\alpha$  from  $35^\circ$  to  $75^\circ$ . They found that the thermohydraulic performance of multiple type V-pattern

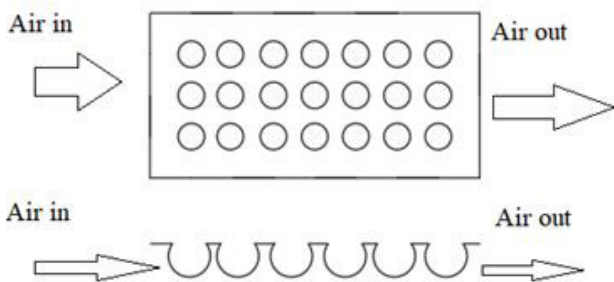


Figure 16. Transverse dimple arrangement.

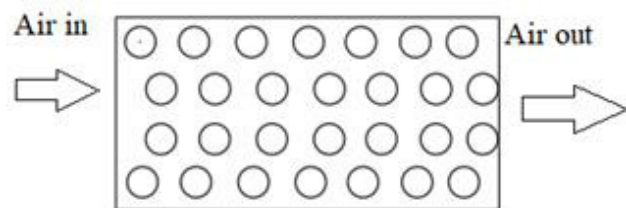


Figure 17. Arc shape dimple arrangement.

dimpled obstacles pattern is around 7.0% more in comparison to other obstacles shapes in air stream path. The best value of thermohydraulic performance was reported to be 3.36 at  $Re$  16000. As a function of coarseness variables and stream variables, correlations for  $Nu$  and friction factor were derived. Configuration used by them is shown in Fig. 18.

#### Hemi-Spherical Protrusion Ribs

##### Staggered protrusion ribs

Bhushan and Singh [63] have been examined the consequence of staggered protrusion ribs and stream variables on heat transfer and friction factor in SAH. The various stream variable and coarseness variable taken into account for the experiment were  $S/e$  from 18.85 to 37.50,  $L/e$  from 25.00 to 37.50,  $d/D$  from 0.147 to 0.367,  $e/D_h$  of 0.03 and  $Re$  from 4000 to 18000. The maximal augmentation in  $Nu$  and friction factor was recorded to be 3.8 and 2.2 folds respectively. The maximal enhancement for  $Nu$  was reported at  $S/e$  of 31.25,  $L/e$  of 31.25 and  $d/D$  of 0.294. As a function of coarseness variables and stream variables, correlations for  $Nu$  and friction factor were derived. Configuration used by them is shown in Fig. 19.

##### Hemi-spherical protrusion in arc shape

Yadav et al. [64] have been examined the consequence of hemi-spherical protrusion in arc shape and stream variables on heat transfer and friction factor in SAH. The various variables taken into account were  $Re$  from 3600 to 18100,  $p/e$  from 12 to 24,  $e/D_h$  from 0.015 to 0.03 and  $\alpha$

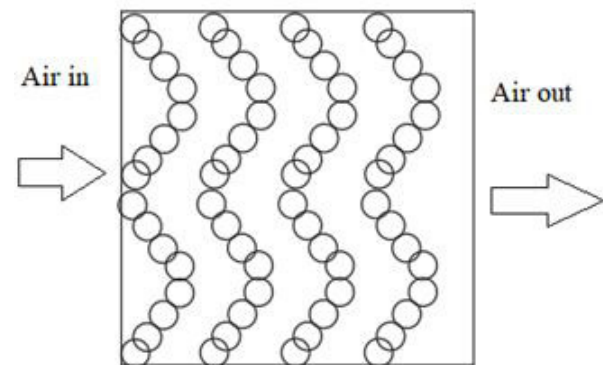


Figure 18. Multiple v dimple arrangement.

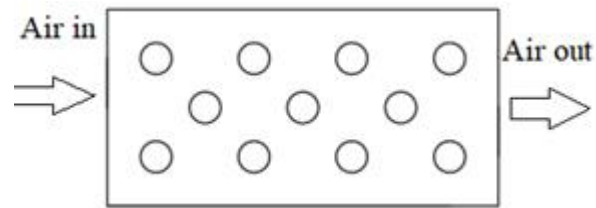


Figure 19. Staggered protrusion ribs.

from 45° to 75°. The maximal augmentation in heat transfer and friction factor was observed to be 2.89 and 2.93 folds respectively. As a function of coarseness variables and stream variables, correlations for Nu and friction factor were derived.

Further, Yadav et al. [65] evaluated the exergetic performance of SAH channel roughened with Hemi-spherical protrusion in arc shape. They found that exergetic efficiency was maximal w.r.t.  $p/e$  of 12,  $e/D_h$  0.03 and  $\alpha$  60° and temperature rise variable 0.02 Km<sup>2</sup>/W.

**Triangular shape protrusion**

Singh et al. [66] have examined the consequence of triangular shape protrusion present over the absorber plate of SAH. The various variable taken into account were Re from 4000 to 20000,  $L/e$  from 18.85–37.5,  $S/e$  from 18.5–37.5 and  $e/D$  of 0.03. They found that the Nusselt number was maximum at  $L/e$  and  $S/e$  of 25 and the friction factor was decrease with increase in  $L/e$  and  $S/e$ . They found that maximum thermohydraulic parameter was evaluated for  $L/e$  and  $S/e$  of 25 with Re of 12000. Configuration used by them was shown in Fig. 20.

**Rib Amalgamations**

**Transverse and inclined ribs amalgamation**

Varun et al. [67] have been examined the consequence of amalgamation of transverse and inclined ribs and operating variables on heat transfer and friction attributes of SAH. The various variables taken into consideration were Re from 2000 to 14 000,  $p/e$  from 3 to 8 and  $e/D_h$  of 0.030. They investigated that the maximum thermal efficiency was obtained w.r.t.  $p/e$  of 8. As a function of coarseness variables and stream variables, correlations for Nu and friction factor were derived. Configuration used by them is shown in Fig. 21.

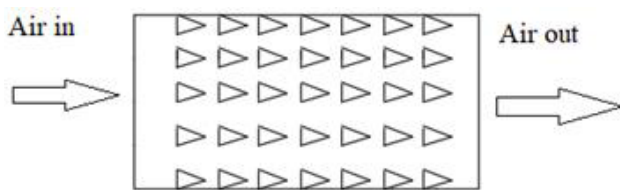


Figure 20. Triangular shaped protrusion.

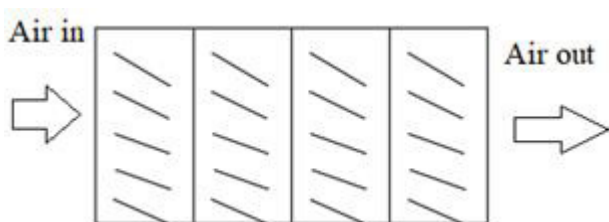


Figure 21. Transverse and inclined ribs combination.

**V shape ribs with gap and staggered ribs amalgamation**

Karwa [68] have been examined the consequence of amalgamation of V shaped ribs with gap and staggered ribs (pointing upward and downward w.r.t. stream) on the heat transfer and friction factor of rectangular channel. The various variables taken into account were the Re from 2800 to 15000,  $e^+$  from 17 to 90,  $e/D_h$  from 0.0467 to 0.05,  $\alpha$  of 60° and  $p/e$  of 10. They observed that the augmentation in the Stanton number was 93–134% and 102–142% for v-up discrete ribs and v-down discrete ribs respectively. The friction factor ratio was found to be 2.35–2.47 and 2.46–2.58 for v-up discrete ribs and v-down discrete ribs respectively.

Patil et al. [69] have been examined the consequence of broken V-rib coarseness amalgamated with staggered ribs on heat transfer and friction factor. The variables taken into consideration were Re from 3000 to 17000,  $s'/s$  from 0.2 to 0.8,  $p'/p$  of 0.6,  $r/e$  of 1,  $p/e$  of 10,  $e/D_h$  of 0.043, Dimensionless gap size 1, and angle of attack 60°. The Nu enhancement ratio and friction factor enhancement ratio reported to be in the span from 1.89–2.85 and 2.05–2.49 respectively. The maximum thermohydraulic performance was found at  $s'/s$  of 0.6.

Later, Patil et al. [70][71] discussed the consequence on heat transfer and friction factor by the variation of coarseness variables. The various variable varied were the Re from 3000 to 17000,  $p'/p$  from 0.2 to 0.8,  $r/e$  from 1 to 2.5,  $s'/s$  from 0.2 to 0.8 for the constant value of  $p/e$  10,  $e/D_h$  of 0.043, Dimensionless gap size of 1 and  $\alpha$  of 60°. The augmentation in Nu lies between 1.77 and 3.18. The maximal value of Nu and friction factor was reported at  $s'/s$  of 0.6,  $p'/p$  of 0.6, and  $r/e$  of 2.5. Optimal thermohydraulic performance has been found w.r.t.  $p'/p$  of 0.6,  $r/e$  of 2.5, and  $s'/s$  of 0.6. As a function of coarseness variables and stream variables, correlations for Nu and friction factor were derived.

Deo et al. [72] have been examined the consequence of multi-gap V down ribs amalgated with staggered ribs on heat transfer and friction factor for SAH. The various variables taken into consideration were the Re from 4000 to 12000,  $p/e$  from 4 to 14,  $e/D_h$  from 0.026 to 0.057,  $\alpha$  from 40° to 80°,  $g/e$  of 1,  $w/e$  of 4.5,  $p/P$  of 0.65. The maximal augmentation in Nu, friction factor and thermohydraulic performance variable was reported to be 3.34, 3.38 and 2.45 times respectively. As a function of coarseness variables and stream variables, correlations for Nu and friction factor were derived.

**Broken arc ribs with staggered ribs**

Gill et al. [73] have been examined the consequence of broken arc shape ribs with staggered ribs on heat transfer and friction factor for SAH. The various variable taken into consideration were the Re from 2000 to 16000,  $p'/p$  of 0.4,  $e/D_h$  of 0.043,  $g/e$  of 1,  $w'/w$  of 0.65,  $\alpha$  of 30°,  $p/e$  of 10,  $r/g$  from 1 to 6. The maximal augmentation in Nu and friction factor was found to be 3.06 and 2.5 times respectively. The maximum thermohydraulic performance occurred at  $r/g$  of 4.

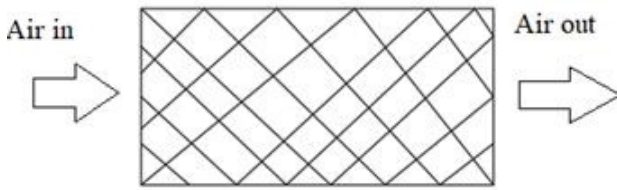


Figure 22. Expanded metal mesh.

### Expanded metal mesh

Sani and Saini [74] have been examined the consequence of expanded metal mesh used on heat transfer and friction factor for SAH. The various stream and coarseness variables taken into consideration were  $Re$  from 1900 to 13000,  $L/e$  from 25 to 71.87,  $S/e$  from 15.62 to 46.87 and  $e/D_h$  from 0.012 to 0.039. The maximal augmentation in heat transfer coefficient and friction factor was determined to be 4 and 5 times respectively. The maximal value of  $Nu$  was attained at  $L/e$  of 46.87,  $S/e$  of 25 and  $\alpha$  of  $61.9^\circ$ . The maximal friction factor was observed at  $\alpha$  of  $72^\circ$  and  $L/e$  of 71.87. As a function of coarseness variables and stream variables, correlations for  $Nu$  and friction factor were derived. Configuration used by them is shown in Fig. 22.

Gupta et al. [75] evaluated EAR, EEAR and EXAR for the various stream variable and coarseness variables used by Saini and Saini [54]. It was reported by them that highest EXAR occurred at  $L/e$  of 40 followed by  $L/e$  of 55. Hence, it was suggested to use  $L/e$  from 40 to 55.

### Metal grit ribs

Karmare and Tikekar [76] have been examined the consequence of metal grit ribs on the heat transfer and friction attributes of SAH. The various stream variable and coarseness variable taken into account were the  $Re$  from 4000 to 17000,  $e/D_h$  from 0.035 to 0.044,  $p/e$  from 12.5 to 36 and  $l/s$  from 1 to 1.72. They observed that the optimum performance of SAH occurred at  $e/D_h$  of 0.044,  $p/e$  of 17.5 and  $l/e$  of 1.72. The maximal augmentation in  $Nu$  and friction factor was observed to be 1.86 and 2.13 times respectively. As a function of coarseness variables and stream variables, correlations for  $Nu$  and friction factor were derived.

Further, Karmare and Tikekar [77] reported that by using metal grit ribs as coarseness component thermal efficiency of SAH was enhanced by 10–35% over SAH with smooth absorber plate.

### Coarseness Produced By Machining

#### Chamfered ribs

Karwa et al. [78] examined the consequence of chamfered ribs on heat transfer and friction attributes of the air in SAH. The various variables taken into account were the  $Re$  from 3000 to 20000,  $W/H$  as 4.8, 6.1, 7.1, 9.66 and 12,  $e/D_h$  from 0.0141 to 0.0328,  $p/e$  from 4.5 to 8.5, rib chamfer angle  $-15^\circ$  to  $18^\circ$ , coarseness Reynolds number from 5 to 60. The maximal value of heat transfer and friction factor

was determined at rib chamfer angle of  $15^\circ$ . As a function of coarseness variables and stream variables, correlations for  $Nu$  and friction factor were derived. Configuration used by them is shown in Fig. 23.

Further, Karwa et al. [79] evaluated the thermohydraulic performance of SAH channel roughened with chamfered ribs. The various variables taken into account were the  $Re$  from 3750 to 16350,  $p/e$  of 4.58 and 7.09 while the rib chamfer angle was kept constant at  $15^\circ$ ,  $e/D_h$  from 0.0197 to 0.0441. The augmentation in thermal efficiency and  $Nu$  was 10 to 40%, 50 to 120% respectively. The friction factor was enhanced from 1.8 to 3.9 times.

#### Wedge shaped ribs

Bhagoria et al. [80] have been examined the consequence of wedge shaped ribs on the heat transfer and friction factor of SAH channel. The various stream and coarseness variables taken into account were the  $Re$  from 3000 to 18000,  $e/D_h$  from 0.015 to 0.033,  $p/e$  from 4.7 to 12.12 and rib wedge angles from  $8^\circ$  to  $15^\circ$ . The augmentation in  $Nu$  and friction factor was determined to be 2.4 and 5.3 times respectively. The maximal value of heat transfer was observed at  $p/e$  of 7.57 and rib wedge angle of  $10^\circ$ . As a function of coarseness variables and stream variables, correlations for  $Nu$  and friction factor were derived. Configuration used by them is shown in Fig. 24.

#### Amalgamation of Machined Coarseness

Jaurker et al. [81] have been examined the consequence of rib-grooved coarseness configuration on the heat transfer and friction attributes. The various variables taken into account during the experimentation were the  $Re$  from 3000 to 21,000,  $e/D_h$  from 0.0181 to 0.0363,  $p/e$  from 4.5 to 10, and  $g/p$  from 0.3 to 0.7. The augmentation in the  $Nu$  and friction factor was observed to be 2.7 and 3.6 times respectively. The maximal value of the heat transfer was reported at  $p/e$  of 10. As a function of coarseness variables

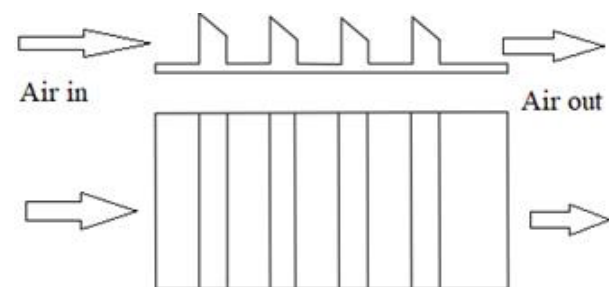


Figure 23. Chamfered ribs.



Figure 24. Wedge shaped ribs.



Figure 25. Transverse ribbed grooved coarseness.

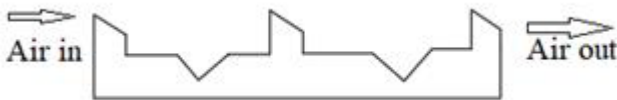


Figure 26. Chamfered ribs and grooved ribs configuration.

and stream variables, correlations for Nu and friction factor were derived. Configuration used by them is shown in Fig. 25.

Layek et al. [82] have been examined the consequence of repeated integral transverse chamfered rib groove coarseness on the heat and fluid stream attributes in SAH. The various variables taken into account were the Re from 3000 to 21000,  $p/e$  from 4.5 to 10, chamfer angle of  $5^\circ$  to  $30^\circ$ ,  $g/p$  from 0.3 to 0.6 and  $e/D_h$  from 0.022 to 0.04. They found that Nu and friction factor enhanced by 3.24 and 3.78 folds as compared to smooth channel. The maximal heat augmentation was observed for the  $p/e$  of 6,  $g/p$  of 0.4 and chamfer angle of  $18^\circ$ . As a function of coarseness variables and stream variables, correlations for Nu and friction factor were derived. Configuration used by them is shown in Fig.38. Further, Layek et al. [83] observed that the entropy generation reduces with rise in  $e/D_h$ . The value of  $p/e$  6,  $g/p$  of 0.4 and chamfer angle of  $18^\circ$  shows the minimal increase in entropy generation. Configuration used by them is shown in Fig. 26.

Layek et al. [84] further, have been examined the consequence of chamfered rib and grooves for the variation in chamfer angles from  $5^\circ$  to  $30^\circ$  while  $p/e$  and  $e/D_h$  were kept constant at 10 and 0.03 respectively. Re was varied from 3000 to 21000. They found that heat transfer and friction factor enhanced by 2.6 and 3.35 folds respectively. The thermohydraulic variable occurred between 1.4 and 1.76 for the investigated geometry.

Summary of various coarseness geometries used by different researchers with the span of variables, findings and correlation developed for Nu and friction factor is shown in appendix A.

### THERMOHYDRAULIC PERFORMANCE VARIABLE FOR VARIOUS ARTIFICIALLY ROUGHENED SURFACES

SAH is said to be effective if maximum heat transfer occurs at minimum power consumption. Thermohydraulic performance in addition to the thermal and hydraulic

performance helps in the choice of SAH model. In this context, thermohydraulic performance helps to determine the optimum value of coarseness variables and geometrical arrangement of ribs. Thermohydraulic performance variable has been determined for the various coarseness used by various investigators using the friction factor correlations and Nu correlations developed by them as given in appendix A. Evaluated span of thermohydraulic performance variable is shown in Table 1 and thermohydraulic performance variable w.r.t. the Reynolds number are compared in Fig. 27.

Fig. 27 shows that thermohydraulic performance variable has broad variety and its value changes from 0.44 to 4.2. Minimal value of thermohydraulic performance variable is reported for the amalgamation of transverse and inclined rib geometry and maximal values are reported for multiple V shaped ribs with gap geometry followed by S shaped ribs. For the S-shaped ribs, thermohydraulic performance is not substantial at low Re, but performance increases drastically at higher Reynolds number.

### COLBURN FACTOR AND FRICTION FACTOR FOR VARIOUS ARTIFICIALLY ROUGHENED SURFACES

The roughened surface gives better heat transfer rate on one hand but on the other hand tends to augment fluid stream friction and pressure drop. Selection of the coarseness geometry is not only carried out on the basis of estimating heat transfer coefficient or dimensionless heat transfer variables like Nu, Stanton number, etc. The main aim is to select such coarseness geometry which gives the augmentation in the heat transfer rate at minimal loss of pumping power. The Colburn  $j$  factor and the friction factor are calculated for various range of Re and the coarseness variables are selected for which various investigator get the maximum thermohydraulic performance. The values of the Colburn  $j$  factor and the friction factor for various coarseness geometries are plotted against Re as shown in Fig. 28 and Fig. 29 respectively.

Fig. 28 shows that the Colburn factor for various coarseness geometries is higher as compare to the smooth surface over the complete span of Re. Only combination of transverse and inclined ribs and metal grit ribs have lower value of Colburn factor below Reynolds number 5000 in comparison to smooth channel. It has been clearly seen from the Fig. 28 that the maximal value of the Colburn factor has been attained by multiple V shaped ribs with gap for the complete span of Re.

Fig. 29 shows the variation of friction factor with the Re. It has been seen that the friction factor reduces with rise in the Re. Friction factor for various coarseness geometries is larger in comparison to the smooth channel. Maximal value of friction factor has been achieved by multiple V shaped ribs below Reynolds number 7500 and maximum value of friction factor has been achieved by discrete V shaped ribs

**Table 1.** Thermohydraulic performance parameter for different artificial coarseness used by various investigators

Investigators	Coarseness configuration	Thermohydraulic performance parameter range
Aharwal et al. [41]	Inclined discrete ribs	1.13–2.22
Momin et al. [42]	Continuous V-shaped ribs	1.12–1.57
Hans et al. [43]	Mutiple V-ribs	2.58–3.58
Lanjewar et al. [45]	W-shaped ribs	1.26–1.58
Kumar et al. [46]	S-Shaped ribs	1.43–4.2
Singh et al. [48]	Discrete V-Down Rib	1.73–1.98
Maithani and Saini [50]	V Shape ribs with symmetrical multiple gap	1.46–1.98
Kumar et al. [52]	Multiple V shape ribs with gap	2.67–3.81
Kumar et al. [53]	Discrete W-shaped ribs	1.41–1.87
Saini and Saini [54]	Arc shape ribs	0.79–2.48
Singh et al. [56]	Multiple arc shape ribs	0.90–2.93
Pandey et al. [58]	Multiple Arc shape ribs with gap	0.80–2.97
Sethi et al. [62]	Arc shape dimple arrangement	0.97–2.09
Bhushan and Singh [64]	Staggered protrusion ribs	0.78–3.37
Yadav et al. [65]	Hemi-spherical protrusion arranged in arc shape	1.75–3.5
Varun et al. [68]	Transverse and Inclined ribs combination	0.44–1.25
Patil et al. [71]	Discrete V ribs combined with staggered ribs	1.38–1.94
Deo et al. [73]	multi-gap V down ribs combined with staggered ribs	1.74–2.45
Saini and Saini [75]	Expanded Metal Mesh	0.69–2.00
Karmare and Tikekar [77]	Metal grit ribs	0.54–1.75
Bhagoria et al. [81]	Wedge shaped rib	0.69–1.69
Jaurker et al. [82]	rib-grooved artificial coarseness	1.46–1.92
Layek et al. [83]	repeated integral transverse chamfered rib groove coarseness	1.82–2.17

with staggered ribs above Reynolds number 7500. From Fig. 29, it can be concluded that the best result for the friction factor for the complete span of the Re is not a single geometry.

Table 2 show the span of friction factor and Colburn factor for coarseness configurations used by various investigators.

## CONCLUSIONS

This article presented the detailed study of different artificial coarseness configuration used by various investigators in SAH. Consequences of different coarseness variables and stream variables on the heat transfer and friction factor have been presented. On the basis of the above discussion, following conclusions have been reported:

1. Providing artificial coarseness to the undersurface of the absorber plate is a good choice for the augmentation of heat transfer in SAH whereas use of artificial coarseness also raises the pumping power requirement.
2. Effect of various coarseness variable and stream variable over the various coarseness configurations were examined.
3.  $e/D_h$ ,  $p/e$  and  $\alpha$  are the coarseness variables which are common to most of the configuration. Almost in the entire configuration the value of Nu and friction factor were determined maximal at  $p/e$  of 8 to 10,  $e/D_h$  of 0.03 and  $\alpha$  of  $60^\circ$ .
4. Creation of gap in continuous ribs increases the heat transfer rate and friction factor while comparing it with that of continuous ribs.
5. Maximum augmentation in the heat transfer occurred by using Multiple V shaped ribs with gap that was followed by S shaped ribs.
6. Maximum augmentation in the friction factor occurred by using Discrete V shaped ribs with staggered ribs that was followed by Multiple V shaped ribs.
7. The maximal value of the Colburn factor was reported by using Multiple V shaped ribs with gap.
8. Correlations for Nu and friction factor developed by different researchers are represented in tabular form.

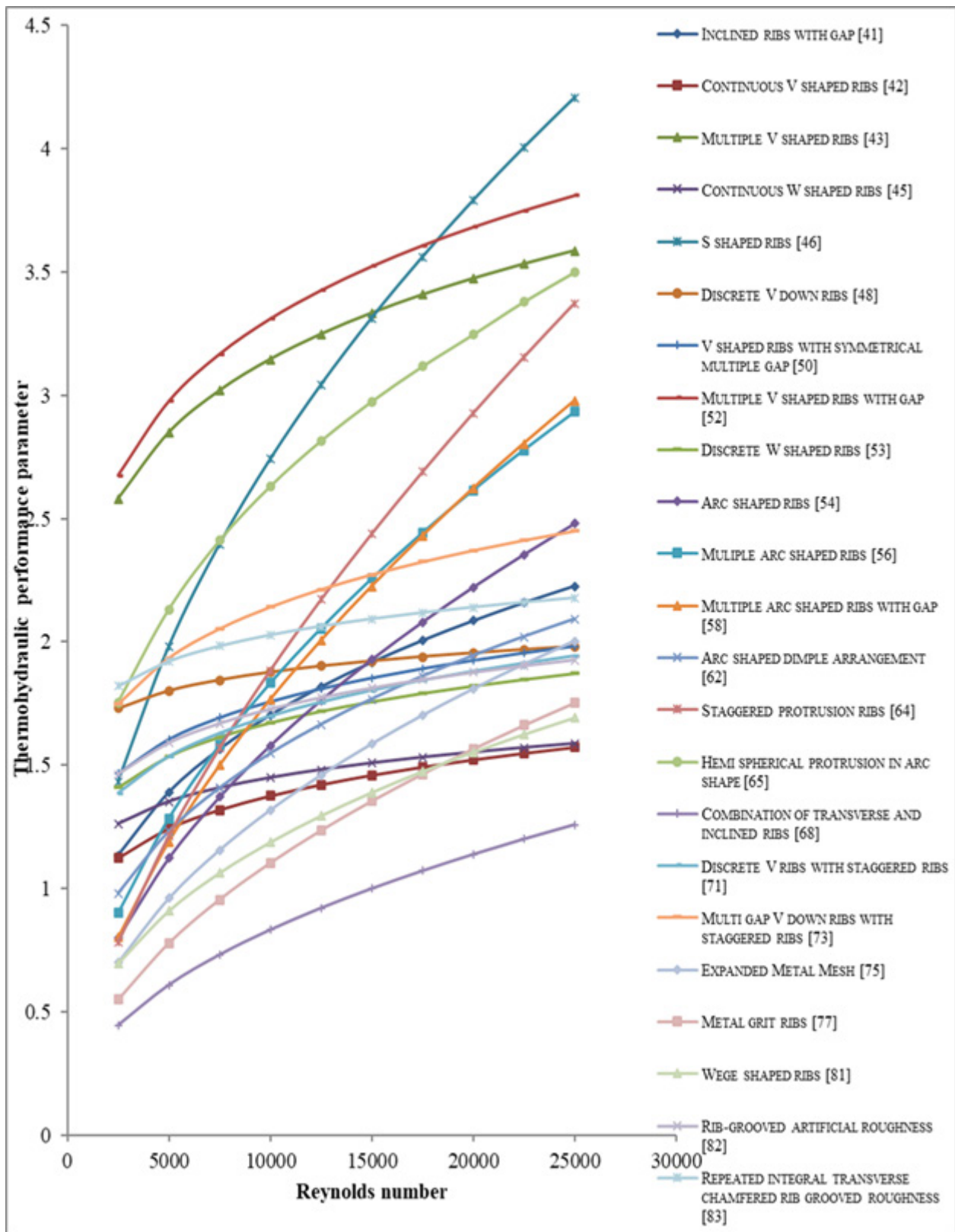


Figure 27. Comparison of Thermohydraulic performance parameter of various coarseness with respect to the Reynolds numbe.

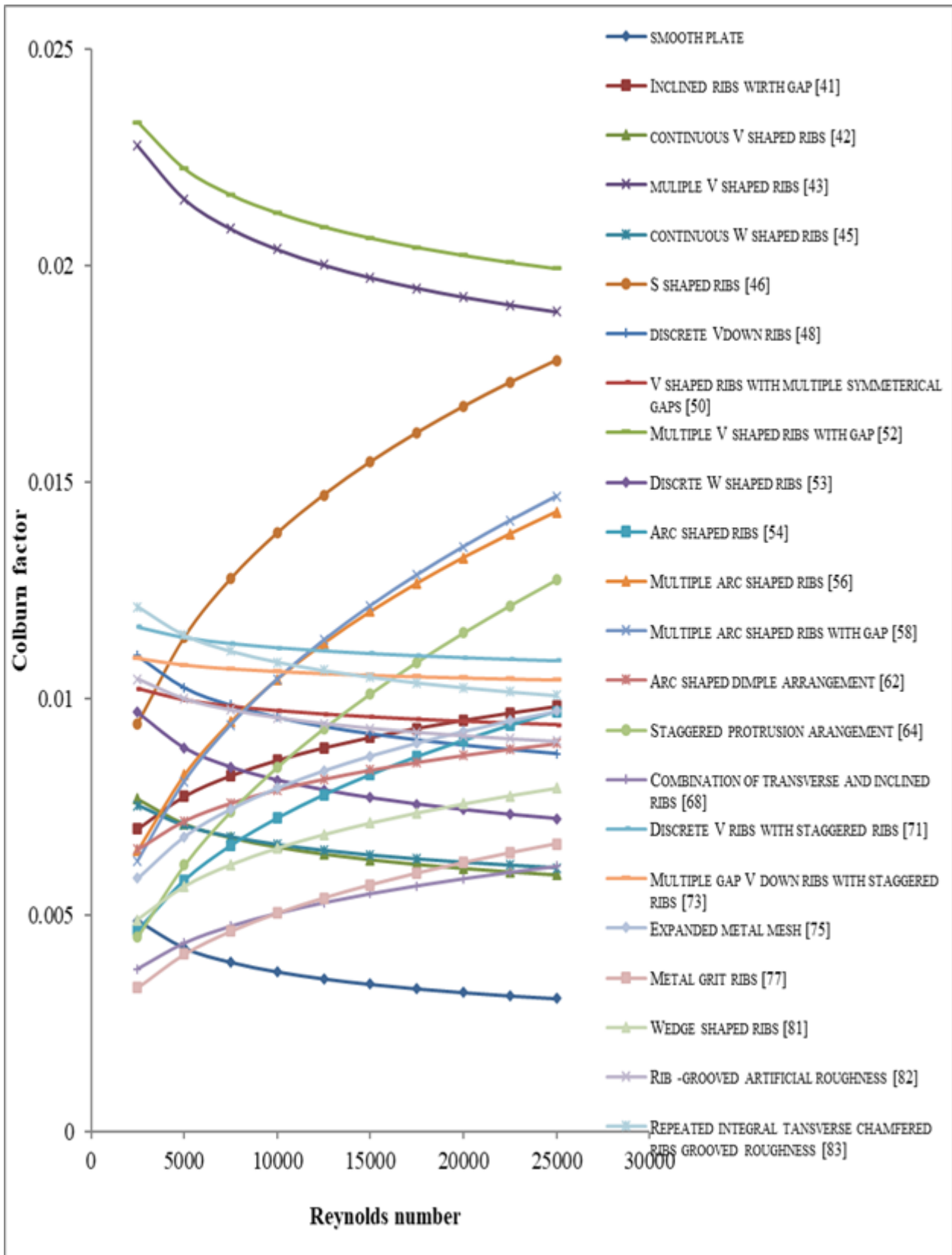


Figure 28. Colburn factor w.r.t Reynolds number.

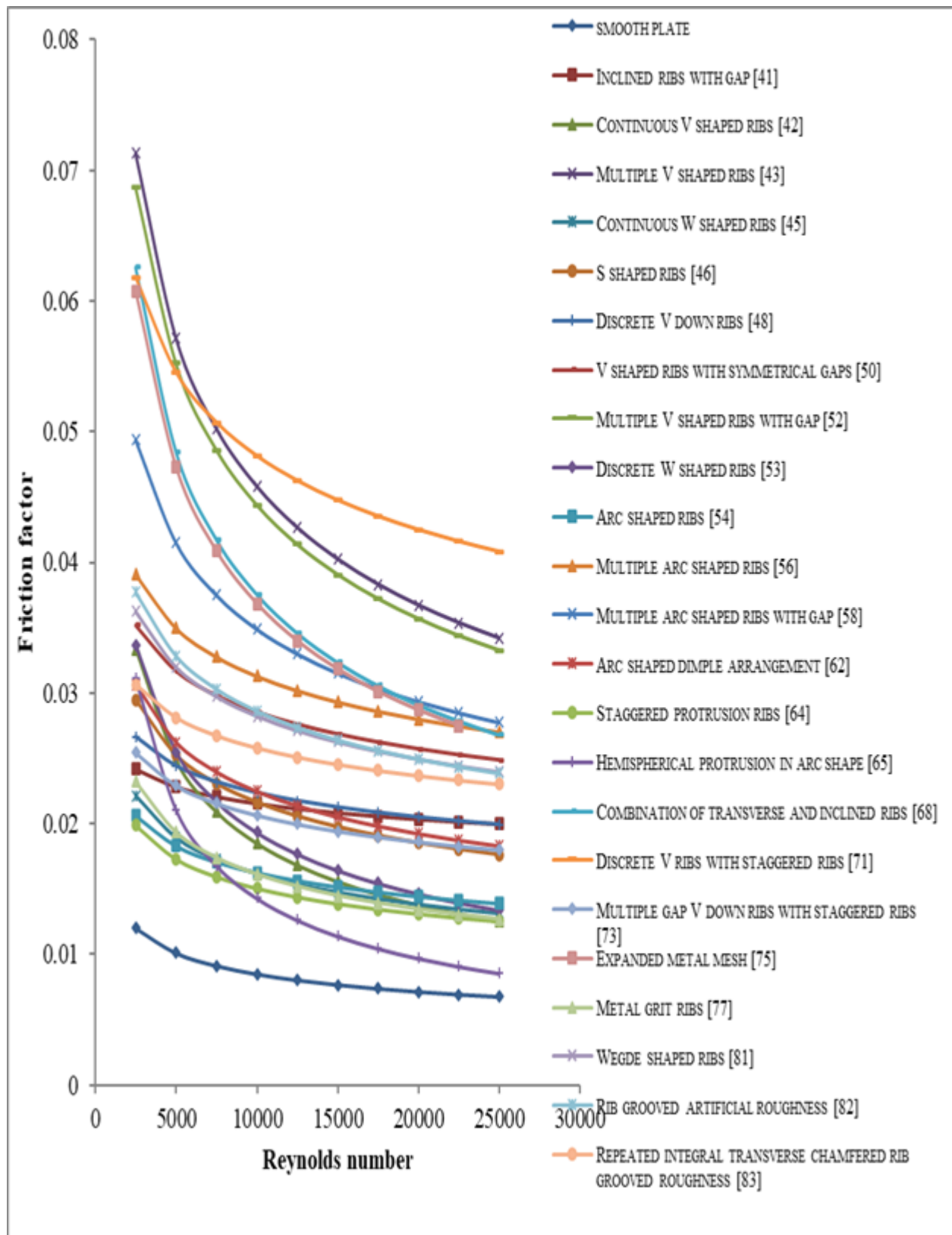


Figure 29. Friction factor w.r.t. Reynolds number.

**Table 2.** Colburn factor and friction factor for different artificial coarseness used by various investigators

Investigators	Coarseness configuration	Colburn factor (J) range	Friction factor (f) range
Aharwal et al. [41]	Inclined discrete ribs	0.006–0.009	0.024–0.019
Momin et al. [42]	Continuous V-shaped ribs	0.007–0.006	0.033–0.012
Hans et al. [43]	Multiple V-ribs	0.022–0.018	0.071–0.034
Lanjewar et al. [45]	W-shaped ribs	0.0075–0.006	0.022–0.013
Kumar et al. [46]	S-Shaped ribs	0.009–0.017	0.029–0.017
Singh et al. [48]	Discrete V-Down Rib	0.01–0.008	0.026–0.019
Maithani and Saini [50]	V Shape ribs with symmetrical multiple gap	0.01–0.0094	0.035–0.024
Kumar et al. [52]	Multiple V shape ribs with gap	0.023–0.0199	0.068–0.033
Kumar et al. [53]	Discrete W-shaped ribs	0.009–0.007	0.033–0.013
Saini and Saini [54]	Arc shape ribs	0.004–0.009	0.020–0.013
Singh et al. [56]	Multiple arc shape ribs	0.006–0.014	0.039–0.027
Pandey et al. [58]	Multiple Arc shape ribs with gap	0.006–0.014	0.049–0.027
Sethi et al. [62]	Arc shape dimple arrangement	0.0065–0.0089	0.030–0.018
Bhushan and Singh [64]	Staggered protrusion ribs	0.004–0.012	0.019–0.012
Varun et al. [68]	Transverse and Inclined ribs combination	0.003–0.006	0.062–0.026
Patil et al. [71]	Discrete V ribs combined with staggered ribs	0.011–0.010	0.061–0.040
Deo et al. [73]	multi-gap V down ribs combined with staggered ribs	0.0109–0.0104	0.025–0.017
Saini and Saini [75]	Expanded Metal Mesh	0.0058–0.0097	0.060–0.026
Karmare and Tikekar [77]	Metal grit ribs	0.003–0.006	0.023–0.012
Bhagoria et al. [81]	Wedge shaped rib	0.004–0.007	0.036–0.023
Jaurker et al. [82]	rib-grooved artificial coarseness	0.01–0.009	0.037–0.023
Layek et al. [83]	repeated integral transverse chamfered rib groove coarseness	0.012–0.01	0.030–0.023

This review article provides the help to the researchers to find the coarseness which provides the maximal augmentation in heat transfer and friction factor for the advancement in the field of SAH. It is very clear that for most of the configurations used by various researchers, the coarseness parameter  $e/D_h$ ,  $p/e$  and  $\alpha$  gives better augmentation in heat transfer and friction factor at 0.03, 8 to 10 and 60° respectively. Hence, different configuration design can be developed for rectangular SAH duct using these coarseness parameters into consideration.

Further, similar configuration of coarseness is recommended to use by changing the duct shape like triangular, hexagonal, etc, so that in future researchers can see the consequence of changing duct shape with similar configuration on the augmentation of the heat transfer and friction factor.

## NOMENCLATURE

SAH Solar Air Heater  
 $e^+$  coarseness Reynolds number  
 Re Reynolds number

$Re(e^+)$  Momentum transfer function  
 $f$  Friction factor  
 EAR Energy Augmentation Ratio  
 EEAR Effective Energy Augmentation Ratio  
 EXAR Exergy Augmentation Ratio  
 $D$  or  $D_h$  Hydraulic diameter, mm  
 $G(e^+)$  Heat transfer function  
 St Stanton number  
 $e/D$  or  $e/D_h$  Dimensionless coarseness height  
 $p/e$  Dimensionless coarseness pitch  
 $W$  Width of channel, mm  
 $H$  Height of channel, mm  
 $W/H$  Aspect ratio  
 $I$  Solar insolation,  $W/m^2$   
 $q_u$  useful heat flux,  $W/m^2$   
 $F_R$  Heat removal factor  
 $U_L$  Overall heat loss coefficient,  $W/m^2K$   
 $T_i$  Inlet temperature, K  
 $T_a$  Ambient temperature, K  
 $T_o$  Outlet temperature, K  
 $\Delta P$  Pressure drop, Pa

L	Long way length of mesh or Length of test section, mm
V	Velocity, m/s
Nu	Nusselt number of roughened channel
$Nu_s$	Nusselt number of smooth channel
$f_s$	friction factor of smooth channel
d	Dimple diameter, mm
e	Rib height, mm
g	Groove position or gap, mm
G	Mass flux, kg/sm <sup>2</sup>
$G_d$	Gap distance, mm
$L_v$	Length of single V-rib
$P'$	Staggered rib position
$s'$	Gap position
S	Short way length of mesh or length of discrete rib
d/W	Dimensionless width of gap
d/x or Gd/Lv	Dimensionless position of gap
d/D	Dimensionless diameter of rib print
g/e	Dimensionless gap position
g/P	Dimensionless groove position
L/e	Dimensionless long way length
p/P	Dimensionless staggered rib pitch
$p'/p$	Dimensionless staggered rib position
r/e or r/g	Dimensionless staggered rib size
$s'/s$	Dimensionless gap position
S/e	Dimensionless short way length
w/e	staggered rib length to rib height ratio
W/w	Dimensionless coarseness width
$W_c/W_d$	Dimensionless dimpled obstacles
$E_d/d_d$	dimpled depth to print diameter
$P_b/e_d$	Dimensionless dimpled pitch
$e_d/D_h$	Dimensionless dimple height
l/s	Dimensionless length of metal grit rib

#### Greek Symbols

$\Phi$	Chamfer angle, degree
$\eta$	Thermohydraulic performance variable
$\eta_{th}$	Thermal efficiency
$\rho$	Density, kg/m <sup>3</sup>
$\alpha$	Angle of attack or arc angle, degree

#### ACKNOWLEDGEMENT

We would like to thank Department of Mechanical Engineering, GLA University, Mathura for providing us all the resources for writing this review paper.

#### AUTHORSHIP CONTRIBUTIONS

Concept, Design and Data Analysis: Gaurav Bharadwaj; Literature search and Writing: Kuwar Mausam; Critical revision: Kamal Sharma.

#### DATA AVAILABILITY STATEMENT

No new data were created in this study. The published publication includes all graphics collected or developed during the study.

#### CONFLICT OF INTEREST

The author declared no potential conflicts of interest with respect to the research, authorship, and/or publication of this article.

#### ETHICS

There are no ethical issues with the publication of this manuscript.

#### REFERENCES

- [1] S.P S. Solar energy : principles of thermal collection and storage. 9th Editio. New Delhi: Tata McGraw-Hill; 2003.
- [2] Varun, Saini RP, Singal SK. A review on roughness geometry used in solar air heaters. Sol Energy 2007;81:1340–50. [\[CrossRef\]](#)
- [3] Kumar A, Saini RP, Saini JS. Heat and fluid flow characteristics of roughened solar air heater ducts - A review. Renew Energy 2012;47:77–94. [\[CrossRef\]](#)
- [4] Yildirim C, Tümen Özdil NF. Theoretical investigation of a solar air heater roughened by ribs and grooves. J Therm Eng 2018;4:1702–12. [\[CrossRef\]](#)
- [5] Minni. Y, Azzi. A ZC and BB. Numerical analysis of turbulent forced-convection flow in a channel with staggered L-shaped baffles. J New Technol Mater 2016;6:44–55.
- [6] Menni Y, Azzi A, Zidani C. Use of waisted triangular-shaped baffles to enhance heat transfer in a constant temperature-surfaced rectangular channel. J Eng Sci Technol 2017;12:3251–73.
- [7] Menni. Y, Chamkha. A. J. LG and BB. Computational fluid dynamical analysis of new obstacle design and its impact on the heat transfer enhancement in a specific type of air flow geometryNo Title. Comput Therm Sci 2018;10:421–47.
- [8] Menni Y, Azzi A. Computational fluid dynamical analysis of turbulent heat transfer in a channel fitted with staggered V-Shaped baffles \*. World J Model Simul 2018;14:108–23.
- [9] Menni Y, Azzi A. Effect of fin spacing on turbulent heat transfer in a channel with cascaded rectangular triangular fins. J New Technol Mater 2017;7:10–21.
- [10] Menni Y. Design and performance evaluation of air solar channels with diverse baffle structures. Comput Therm Sci 10AD;3:225–49.

- [11] Menni Y, Chamkha A, Zidani C, Benyoucef B. Baffle orientation and geometry effects on turbulent heat transfer of a constant property incompressible fluid flow inside a rectangular channel. *Int J Numer Methods Heat Fluid Flow* 2020;30:3027–52. [CrossRef]
- [12] Menni Y, Azzi, A. and CA. Developing heat transfer in a solar air channel with arc-shaped baffles: effect of baffle attack angle. *J New Technol Mater* 2018;8:58–67.
- [13] Menni Y, Azzi A, Chamkha A. Enhancement of convective heat transfer in smooth air channels with wall-mounted obstacles in the flow path: A review. *J Therm Anal Calorim* 2019;135:1951–76. [CrossRef]
- [14] Menni Y, Azzi A, Chamkha A. A review of solar energy collectors: Models and applications. *J Appl Comput Mech* 2018;4:375–401. [CrossRef]
- [15] Menni Y, Azzi A, Chamkha AJ, Harmand S. Effect of wall-mounted V-baffle position in a turbulent flow through a channel: Analysis of best configuration for optimal heat transfer. *Int J Numer Methods Heat Fluid Flow* 2019;29:3908–37. [CrossRef]
- [16] Menni Y, Azzi A, Chamkha AJ, Harmand S. Analysis of fluid dynamics and heat transfer in a rectangular duct with staggered baffles. *J Appl Comput Mech* 2019;5:231–48. [CrossRef]
- [17] Menni Y, Azzi A, Chamkha AJ. The solar air channels: Comparative analysis, introduction of arc-shaped fins to improve the thermal transfer. *J Appl Comput Mech* 2019;5:616–26. [CrossRef]
- [18] Menni Y, Azzi A, Chamkha A. Modeling and analysis of solar air channels with attachments of different shapes. *Int J Numer Methods Heat Fluid Flow* 2019;29:1815–45. [CrossRef]
- [19] Menni Y, Chamkha AJ, Azzi A. Fluid flow and heat transfer over staggered + shaped obstacles. *J Appl Comput Mech* 2020;6:741–56. [CrossRef]
- [20] Menni Y, Chamkha AJ, Zidani C, Benyoucef B. Analysis of thermo-hydraulic performance of a solar air heater tube with modern obstacles. *Arch Thermodyn* 2020;41:33–56. [CrossRef]
- [21] Menni Y, Chamkha AJ, Zidani C. Computational thermal analysis of turbulent forced-convection flow in an air channel with a flat rectangular fin and downstream v-shaped baffle. *Heat Transf Res* 2019;50:1781–818.
- [22] Menni Y, Azzi A, Zidani C. A numerical study of momentum and forced convection heat transfer in a rectangular channel with wall-mounted waved baffles. *Rev Des Sci La Technol* 2016;33:1–15.
- [23] Menni Y. Numerical analysis of turbulent forced convection in a channel with flat and diamond-shaped baffles of different heights. *Courr Du Savoir* 2017;23:75–84.
- [24] Menni Y, Azzi A, Zidani C. Computational analysis of turbulent forced convection in a channel with staggered corrugated baffles. *Commun Sci Technol* 2016;16:34–43.
- [25] Bhatti. M, Shah. R. Turbulent and transition stream convective heat transfer in ducts. New York: John Willey & Sons; 1987.
- [26] Dippery. S, Sabersky. R. No THeat and momentum transfer in smooth and rough tubes at various Prandtl numbers. *Int J Heat Mass Transf* 1963;36:1459–69.
- [27] Gee DL, Webb RL. Forced convection heat transfer in helically rib-roughened tubes. *Int J Heat Mass Transf* 1980;23:1127–36. [CrossRef]
- [28] Garg. H, Prakash. J. Solar energy fundamentals and applications. Tata McGraw-Hill; 1997.
- [29] Duffie. J, Beckmen. W. Solar engineering of thermal processes. Wiley, New York; 1980.
- [30] Frank. K, Raj. M, Mark. S. Principles of heat transfer. Global Engineering: Christopher M. Shortt; 2003.
- [31] Lewis MJ. Optimising the thermohydraulic performance of rough surfaces. *Int J Heat Mass Transf* 1975;18:1243–8. [CrossRef]
- [32] Saini JS. Effect of artificial roughness on heat transfer and friction factor in a solar air heater 1988;41:555–60.
- [33] Taslim, M.E.; Li, T.; Kercher DM. Experimental Heat Transfer and Opposite Walls. *J Turbomach* 1996;118:20–8.
- [34] Aharwal KR, Gandhi BK, Saini JS. Experimental investigation on heat-transfer enhancement due to a gap in an inclined continuous rib arrangement in a rectangular duct of solar air heater. *Renew Energy* 2008;33:585–96. [CrossRef]
- [35] Ahn SW. The effects of roughness types on friction factors and heat transfer in roughened rectangular duct. *Int Commun Heat Mass Transf* 2001;28:933–42. [CrossRef]
- [36] Prasad BN, Saini JS. Optimal Thermohydraulic Performance. *Sol Energy* 1991;47:91–6.
- [37] Gupta D, Solanki SC, Saini JS. Heat and fluid flow in rectangular solar air heater ducts having transverse rib roughness on absorber plates. *Sol Energy* 1993;51:31–7. [CrossRef]
- [38] Verma SK, Prasad BN. Investigation for the optimal thermohydraulic performance of artificially roughened solar air heaters. *Renew Energy* 2000;20:19–36. [CrossRef]
- [39] Sahu MM, Bhagoria JL. Augmentation of heat transfer coefficient by using 90° broken transverse ribs on absorber plate of solar air heater. *Renew Energy* 2005;30:2057–73. [CrossRef]
- [40] Gupta D, Solanki SC, Saini JS. Thermohydraulic performance of solar air heaters with roughened absorber plates. *Sol Energy* 1997;61:33–42. [CrossRef]
- [41] Aharwal KR, Gandhi BK, Saini JS. Heat transfer and friction characteristics of solar air heater ducts

- having integral inclined discrete ribs on absorber plate. *Int J Heat Mass Transf* 2009;52:5970–7. [\[CrossRef\]](#)
- [42] Lanjewar A, Bhagoria JL, Sarviya RM. Heat transfer and friction in solar air heater duct with W-shaped rib roughness on absorber plate. *Energy* 2011;36:4531–41. [\[CrossRef\]](#)
- [43] Hans VS, Saini RP, Saini JS. Heat transfer and friction factor correlations for a solar air heater duct roughened artificially with multiple v-ribs. *Sol Energy* 2010;84:898–911. [\[CrossRef\]](#)
- [44] Lanjewar AM, Bhagoria JL, Sarviya RM. Performance analysis of W-shaped rib roughened solar air heater. *J Renew Sustain Energy* 2011;3:1–11. [\[CrossRef\]](#)
- [45] Kumar K, Prajapati DR, Samir S. Heat transfer and friction factor correlations development for solar air heater duct artificially roughened with ‘S’ shape ribs. *Exp Therm Fluid Sci* 2017;82:249–61. [\[CrossRef\]](#)
- [46] Singh S, Chander S, Saini JS. Investigations on thermo-hydraulic performance due to flow-attack-angle in V-down rib with gap in a rectangular duct of solar air heater. *Appl Energy* 2012;97:907–12. [\[CrossRef\]](#)
- [47] Singh S, Chander S, Saini JS. Heat transfer and friction factor correlations of solar air heater ducts artificially roughened with discrete V-down ribs. *Energy* 2011;36:5053–64. [\[CrossRef\]](#)
- [48] Singh S, Chander S, Saini JS. Thermal and effective efficiency based analysis of discrete V-down rib-roughened solar air heaters. *J Renew Sustain Energy* 2011;3. [\[CrossRef\]](#)
- [49] Maithani R, Saini JS. Heat transfer and friction factor correlations for a solar air heater duct roughened artificially with V-ribs with symmetrical gaps. *Exp Therm Fluid Sci* 2016;70:220–7. [\[CrossRef\]](#)
- [50] Kumar A, Saini RP, Saini JS. Experimental investigation on heat transfer and fluid flow characteristics of air flow in a rectangular duct with Multi v-shaped rib with gap roughness on the heated plate. *Sol Energy* 2012;86:1733–49. [\[CrossRef\]](#)
- [51] Kumar A, Saini RP, Saini JS. Development of correlations for Nusselt number and friction factor for solar air heater with roughened duct having multi v-shaped with gap rib as artificial roughness. *Renew Energy* 2013;58:151–63. [\[CrossRef\]](#)
- [52] Kumar A, Bhagoria JL, Sarviya RM. Heat transfer and friction correlations for artificially roughened solar air heater duct with discrete W-shaped ribs. *Energy Convers Manag* 2009;50:2106–17. [\[CrossRef\]](#)
- [53] Saini SK, Saini RP. Development of correlations for Nusselt number and friction factor for solar air heater with roughened duct having arc-shaped wire as artificial roughness. *Sol Energy* 2008;82:1118–30. [\[CrossRef\]](#)
- [54] Sahu MK, Prasad RK. Exergy based performance evaluation of solar air heater with arc-shaped wire roughened absorber plate. *Renew Energy* 2016;96:233–43. [\[CrossRef\]](#)
- [55] Singh AP, Varun, Siddhartha. Heat transfer and friction factor correlations for multiple arc shape roughness elements on the absorber plate used in solar air heaters. *Exp Therm Fluid Sci* 2014;54:117–26. [\[CrossRef\]](#)
- [56] Singh AP, Varun, Siddhartha. Effect of artificial roughness on heat transfer and friction characteristics having multiple arc shaped roughness element on the absorber plate. *Sol Energy* 2014;105:479–93. [\[CrossRef\]](#)
- [57] Pandey NK, Bajpai VK, Varun. Experimental investigation of heat transfer augmentation using multiple arcs with gap on absorber plate of solar air heater. *Sol Energy* 2016;134:314–26. [\[CrossRef\]](#)
- [58] Pandey NK, Bajpai VK. Thermo-hydraulic performance enhancement of solar air heater (SAH) having multiple arcs with gap shaped roughness element on absorber plate. *Int J Eng Sci Technol* 2016;8:34–42. [\[CrossRef\]](#)
- [59] Saini RP, Verma J. Heat transfer and friction factor correlations for a duct having dimple-shape artificial roughness for solar air heaters. *Energy* 2008;33:1277–87. [\[CrossRef\]](#)
- [60] Sethi M, Thakur NS, Varun. Heat transfer and friction characteristics of dimple-shaped roughness element arranged in angular fashion (arc) on the absorber plate of solar air heater. *J Renew Sustain Energy* 2012;4. [\[CrossRef\]](#)
- [61] Sethi M, Varun, Thakur NS. Correlations for solar air heater duct with dimpled shape roughness elements on absorber plate. *Sol Energy* 2012;86:2852–61. [\[CrossRef\]](#)
- [62] Kumar A, Kumar R, Maithani R, Chauhan R, Sethi M, Kumari A, et al. Correlation development for Nusselt number and friction factor of a multiple type V-pattern dimpled obstacles solar air passage. *Renew Energy* 2017;109:461–79. [\[CrossRef\]](#)
- [63] Bhushan B, Singh R. Nusselt number and friction factor correlations for solar air heater duct having artificially roughened absorber plate. *Sol Energy* 2011;85:1109–18. [\[CrossRef\]](#)
- [64] Yadav S, Kaushal M, Varun, Siddhartha. Nusselt number and friction factor correlations for solar air heater duct having protrusions as roughness elements on absorber plate. *Exp Therm Fluid Sci* 2013;44:34–41. [\[CrossRef\]](#)
- [65] Yadav S, Kaushal M, Varun, Siddhartha. Exergetic performance evaluation of solar air heater having arc shape oriented protrusions as roughness element. *Sol Energy* 2014;105:181–9. [\[CrossRef\]](#)
- [66] Singh J, Singh R, Bhushan B. Thermo Hydraulic Performance of Solar Air Duct Having. *J Therm Eng* 2015;1(7):607–320.

- [67] Varun, Saini RP, Singal SK. Investigation of thermal performance of solar air heater having roughness elements as a combination of inclined and transverse ribs on the absorber plate. *Renew Energy* 2008;33:1398–405. [CrossRef]
- [68] Karwa R. Experimental studies of augmented heat transfer and friction in asymmetrically heated rectangular ducts with ribs on the heated wall in transverse, inclined, v-continuous and v-discrete pattern. *Int Commun Heat Mass Transf* 2003;30:241–50. [CrossRef]
- [69] Patil AK, Saini JS, Kumar K. Effect of gap position in broken V-rib roughness combined with staggered rib on thermohydraulic performance of solar air heater. *Green* 2011;1:329–38. [CrossRef]
- [70] Patil AK, Saini JS, Kumar K. Heat transfer and friction characteristics of solar air heater duct roughened by broken V-shape ribs combined with staggered rib piece. *J Renew Sustain Energy* 2012;4. [CrossRef]
- [71] Patil AK, Saini JS, Kumar K. Nusselt number and friction factor correlations for solar air heater duct with broken V-down ribs combined with staggered rib roughness. *J Renew Sustain Energy* 2012;4. [CrossRef]
- [72] Deo NS, Chander S, Saini JS. Performance analysis of solar air heater duct roughened with multigap V-down ribs combined with staggered ribs. *Renew Energy* 2016;91:484–500. [CrossRef]
- [73] Gill RS, Hans VS, Saini JS, Singh S. Investigation on performance enhancement due to staggered piece in a broken arc rib roughened solar air heater duct. *Renew Energy* 2017;104:148–62. [CrossRef]
- [74] Saini RP, Saini JS. Heat transfer and friction factor correlations for artificially roughened ducts with expanded metal mesh as roughness element. *Int J Heat Mass Transf* 1997;40:973–86. [CrossRef]
- [75] Gupta MK, Kaushik SC. Performance evaluation of solar air heater having expanded metal mesh as artificial roughness on absorber plate. *Int J Therm Sci* 2009;48:1007–16. [CrossRef]
- [76] Karmare S V, Tikekar AN. Heat transfer and friction factor correlation for artificially roughened duct with metal grit ribs. *Int J Heat Mass Transf* 2007;50:4342–51. [CrossRef]
- [77] Karmare S V, Tikekar AN. Experimental investigation of optimum thermohydraulic performance of solar air heaters with metal rib grits roughness. *Sol Energy* 2009;83:6–13. [CrossRef]
- [78] Karwa R, Solanki SC, Saini JS. Heat transfer coefficient and friction factor correlations for the transitional flow regime in rib-roughened rectangular ducts. *Int J Heat Mass Transf* 1999;42:1597–615. [CrossRef]
- [79] Karwa R, Solanki SC, Saini JS. Thermo-hydraulic performance of solar air heaters having integral chamfered rib roughness on absorber plates. *Energy* 2001;26:161–76. [CrossRef]
- [80] Bhagoria JL, Saini JS, Solanki SC. Heat transfer coefficient and friction factor correlations for rectangular solar air heater duct having transverse wedge shaped rib roughness on the absorber plate. *Renew Energy* 2002;25:341–69. [CrossRef]
- [81] Jaurker AR, Saini JS, Gandhi BK. Heat transfer and friction characteristics of rectangular solar air heater duct using rib-grooved artificial roughness. *Sol Energy* 2006;80:895–907. [CrossRef]
- [82] Layek A, Saini JS, Solanki SC. Heat transfer and friction characteristics for artificially roughened ducts with compound turbulators. *Int J Heat Mass Transf* 2007;50:4845–54. [CrossRef]
- [83] Layek A, Saini JS, Solanki SC. Second law optimization of a solar air heater having chamfered rib-groove roughness on absorber plate. *Renew Energy* 2007;32:1967–80. [CrossRef]
- [84] Layek A, Saini JS, Solanki SC. Effect of chamfering on heat transfer and friction characteristics of solar air heater having absorber plate roughened with compound turbulators. *Renew Energy* 2009;34:1292–8. [CrossRef]

APPENDIX A

Summary of coarseness used with the range of parameters and developed Correlations				
Investigators	Coarseness configuration	Range of parameters	Findings	Correlations
Prasad and Saini [32]	Continuous transverse ribs	Re = 5000-50000 e/D <sub>h</sub> = 0.02-0.033 p/e = 10-20	$Nu_r = 2.53Nu_s$ $f_r = 4.25f_s$	-----
Gupta et. al.[37]	Continuous transverse ribs	Re=3000-18000 e/D=0.018-0.052 p/e=10 W/H = 6.8-11.5 e <sup>+</sup> = 5-70	-----	<p>For e<sup>+</sup> &lt; 35</p> $Nu = 0.000824 \times \left(\frac{e}{D}\right)^{0.178} \left(\frac{W}{H}\right)^{0.288} Re^{1.062}$ <p>For e<sup>+</sup> ≥ 35</p> $Nu = 0.00307 \times \left(\frac{e}{D}\right)^{-0.469} \left(\frac{W}{H}\right)^{0.245} Re^{0.812}$ $f = 0.06412 \times (e/D)^{0.019} Re^{-0.185} (W/H)^{0.237}$
Verma and Prasad [38]	Continuous transverse ribs	Re=5000-20000 e/D=0.01-0.03 p/e=10-40 e <sup>+</sup> = 8-42	$Nu_r = 2.16Nu_s$	<p>For e<sup>+</sup> ≤ 24</p> $Nu = 0.08596 \times \left(\frac{e}{D}\right)^{0.072} \left(\frac{p}{e}\right)^{0.054} Re^{0.723}$ <p>For e<sup>+</sup> &gt; 24</p> $Nu = 0.02954 \times \left(\frac{e}{D}\right)^{0.021} \left(\frac{p}{e}\right)^{-0.016} Re^{0.802}$ $f = 0.245 \times \left(\frac{e}{D}\right)^{0.203} \left(\frac{p}{e}\right)^{-0.206} Re^{-1.25}$
Sahu and Bhagoria [39]	Broken transverse ribs	Re = 3000-12000 P = 10-30mm e/D = 0.0338	$h_r = (1.25 \text{ to } 1.4)h_s$	-----

Gupta et al. [40]	Continuous inclined ribs	Re=3000-18000 e/D=0.018-0.052 p/e=10 W/H = 6.8-11.5 $\alpha = 60^\circ$	$\eta = (1.16 \text{ to } 1.25)\eta_s$	-----
Aharwal et al. [41]	Inclined discrete ribs	Re = 3000-18000 e/D <sub>h</sub> = 0.018-0.037 p/e = 4-10 d/W = 0.16-0.5 g/e = 0.5-2 $\alpha = 30^\circ-90^\circ$	$Nu = 2.83Nu_s$ $f = 3.60f_s$	$Nu = 0.0102 \times Re^{1.148} \left(\frac{e}{D_h}\right)^{0.51} \left[1 - \left(0.25 - \frac{d}{W}\right)^2 \times \left\{0.01 \times \left(1 - \frac{g}{e}\right)^2\right\}\right]$ $f = 0.5 \times Re^{-0.0836} \left(e/D_h\right)^{0.72}$
Momin et al. [42]	Continuous V-shaped ribs	Re = 2500-18000 p/e = 10 e/D <sub>h</sub> = 0.02-0.034 $\alpha = 30^\circ-90^\circ$	$Nu = 2.3Nu_s$ $f = 2.83f_s$	$Nu = 0.067 \times Re^{0.888} \left(\frac{\alpha}{60}\right)^{-0.077} \left(\frac{e}{D_h}\right)^{0.424} \exp\left[-0.782 \left\{\ln\left(\frac{\alpha}{60}\right)\right\}^2\right]$ $f = 6.266 \times Re^{-0.425} \left(\frac{\alpha}{60}\right)^{-0.093} \left(\frac{e}{D_h}\right)^{0.565} \exp\left[-0.719 \left\{\ln\left(\frac{\alpha}{60}\right)\right\}^2\right]$
Hans et al. [43]	Mutiple V-ribs	Re = 2000-20000 p/e = 6-12 e/D = 0.019-0.043 $\alpha = 30^\circ-75^\circ$ W/w = 1-10	$Nu = 6Nu_s$ $f = 5f_s$	$Nu = 3.35 \times 10^{-5} \times Re^{0.92} \left(\frac{e}{D}\right)^{0.77} \left(\frac{W}{w}\right)^{0.43} \left(\frac{\alpha}{90}\right)^{-0.49}$ $\exp\left[-0.1177 \left\{\ln\left(\frac{W}{w}\right)\right\}^2\right] \exp\left[-0.61 \left\{\ln\left(\frac{\alpha}{90}\right)\right\}^2\right] \left(\frac{p}{e}\right)^{8.54}$ $\exp\left[-2.0407 \left\{\ln\left(\frac{p}{e}\right)\right\}^2\right]$ $f = 4.47 \times 10^{-4} \times Re^{-0.3188} \left(\frac{e}{D}\right)^{0.73} \left(\frac{W}{w}\right)^{0.22} \left(\frac{\alpha}{90}\right)^{-0.39}$ $\exp\left[-0.52 \left\{\ln\left(\frac{\alpha}{90}\right)\right\}^2\right] \left(\frac{p}{e}\right)^{8.9} \exp\left[-2.133 \left\{\ln\left(\frac{p}{e}\right)\right\}^2\right]$

Lanjewar et. al. [45]	W-shaped ribs	Re = 2300-14000 p/e = 10 e/D <sub>h</sub> = 0.018-0.03375 α = 30°-75°	<b>Nu = 2.36Nu<sub>s</sub></b> <b>f = 2.01f<sub>s</sub></b>	$Nu = 0.0613 \times Re^{0.9079} \left(\frac{e}{D_h}\right)^{0.4487} \left(\frac{\alpha}{60}\right)^{-0.1331}$ $\exp\left[-0.5307\left\{\ln\left(\frac{\alpha}{60}\right)\right\}^2\right]$ $f = 0.6182 \times Re^{-0.2254} \left(\frac{e}{D_h}\right)^{0.4622} \left(\frac{\alpha}{60}\right)^{-0.0817}$ $\exp\left[-0.28\left\{\ln\left(\frac{\alpha}{60}\right)\right\}^2\right]$
Kumar et. al. [46]	S-Shaped ribs	Re = 2400-20000 p/e = 4-16 e/D <sub>h</sub> = 0.022-0.054 α = 30°-75° W/w = 1-4	<b>Nu = 4.64Nu<sub>s</sub></b> <b>f = 2.71f<sub>s</sub></b>	$Nu = 1.4332 \times 10^{-4} \times Re^{1.2764} \left(\frac{W}{w}\right)^{0.2748} \exp\left[-0.1084\left\{\ln\left(\frac{W}{w}\right)\right\}^2\right]$ $\left(\frac{p}{e}\right)^{0.4876} \exp\left[-0.1107\left\{\ln\left(\frac{p}{e}\right)\right\}^2\right] \left(\frac{\alpha}{90}\right)^{-0.0468}$ $\exp\left[-0.0642\left\{\ln\left(\frac{\alpha}{90}\right)\right\}^2\right] \left(\frac{e}{D_h}\right)^{-0.7653}$ $f = 1.430 \times 10^{-1} \times Re^{-0.224} \left(\frac{W}{w}\right)^{0.1424} \left(\frac{p}{e}\right)^{0.7657}$ $\exp\left[-0.187\left\{\ln\left(\frac{p}{e}\right)\right\}^2\right] \left(\frac{\alpha}{90}\right)^{0.2129} \left(\frac{e}{D_h}\right)^{0.2159}$
Singh et. al. [48]	Discrete V-Down Rib	Re = 3000-15000 p/e = 4-12 e/D <sub>h</sub> = 0.015-0.043 α = 30°-75° g/e = 0.5-2 d/w = 0.2-0.8	<b>Nu = 3.04Nu<sub>s</sub></b> <b>f = 3.11f<sub>s</sub></b>	$Nu = 2.36 \times 10^{-3} \times Re^{0.9} \left(\frac{p}{e}\right)^{3.5} \left(\frac{\alpha}{60}\right)^{-0.023} \left(\frac{d}{w}\right)^{-0.043} \left(\frac{g}{e}\right)^{-0.014}$ $\left(\frac{e}{D_h}\right)^{0.47} \exp\left[-0.84\left\{\ln\left(\frac{p}{e}\right)\right\}^2\right] \exp\left[-0.72\left\{\ln\left(\frac{\alpha}{60}\right)\right\}^2\right]$ $\exp\left[-0.05\left\{\ln\left(\frac{d}{w}\right)\right\}^2\right] \exp\left[-0.15\left\{\ln\left(\frac{g}{e}\right)\right\}^2\right]$

				$f = 4.13 \times 10^{-2} \times Re^{-0.126} \left(\frac{p}{e}\right)^{2.74} \left(\frac{\alpha}{60}\right)^{-0.034} \left(\frac{d}{w}\right)^{-0.058} \left(\frac{g}{e}\right)^{0.031}$ $\left(\frac{e}{D_h}\right)^{0.7} \exp\left[-0.685 \left\{\ln\left(\frac{p}{e}\right)\right\}^2\right] \exp\left[-0.93 \left\{\ln\left(\frac{\alpha}{60}\right)\right\}^2\right]$ $\exp\left[-0.058 \left\{\ln\left(\frac{d}{w}\right)\right\}^2\right] \exp\left[-0.21 \left\{\ln\left(\frac{g}{e}\right)\right\}^2\right]$
Maithani and Saini [50]	V Shape ribs with symmetrical multiple gap	<p>Re = 4000-18000  p/e = 6-12  e/D = 0.043  α = 30°-75°  g/e = 1-5  N<sub>g</sub> = 1-5</p>	<p><b>Nu = 3.6Nu<sub>s</sub></b>  <b>f = 3.67f<sub>s</sub></b></p>	$Nu = 1.8 \times 10^{-6} \times Re^{0.9635} N_g^{0.126} \left(\frac{g}{e}\right)^{0.111} \left(\frac{p}{e}\right)^{5.7419} \left(\frac{\alpha}{60}\right)^{0.1307}$ $\exp\left[-0.055 \left\{\ln(N_g)\right\}^2\right] \exp\left[-0.0401 \left\{\ln\left(\frac{g}{e}\right)\right\}^2\right] \exp\left[-1.299 \left\{\ln\left(\frac{p}{e}\right)\right\}^2\right]$ $\exp\left[-0.895 \left\{\ln\left(\frac{\alpha}{60}\right)\right\}^2\right]$ $f = 3.6 \times 10^{-7} \times Re^{-0.1512} N_g^{0.1484} \left(\frac{g}{e}\right)^{0.072} \left(\frac{p}{e}\right)^{9.24} \left(\frac{\alpha}{60}\right)^{0.07}$ $\exp\left[-0.0763 \left\{\ln(N_g)\right\}^2\right] \exp\left[-0.0249 \left\{\ln\left(\frac{g}{e}\right)\right\}^2\right] \exp\left[-2.08 \left\{\ln\left(\frac{p}{e}\right)\right\}^2\right]$ $\exp\left[-0.3364 \left\{\ln\left(\frac{\alpha}{60}\right)\right\}^2\right]$
Kumar et. al. [52]	Multiple V shape ribs with gap	<p>Re = 2000-20000  p/e = 6-12  e/D = 0.019-0.043  α = 30°-75°  W/w = 1-10  Gd/Lv = 0.24-0.8  g/e = 0.5-1.5</p>	<p><b>Nu = 6.74Nu<sub>s</sub></b>  <b>f = 6.37f<sub>s</sub></b></p>	$Nu = 0.008532 \times Re^{0.932} \left(\frac{e}{D}\right)^{0.175} \left(\frac{W}{w}\right)^{0.506} \left(\frac{Gd}{Lv}\right)^{-0.0348} \left(\frac{p}{e}\right)^{1.196}$ $\exp\left[-0.0753 \left\{\ln\left(\frac{W}{w}\right)\right\}^2\right] \exp\left[-0.0653 \left\{\ln\left(\frac{Gd}{Lv}\right)\right\}^2\right] \left(\frac{g}{e}\right)^{-0.0708}$ $\left(\frac{\alpha}{60}\right)^{-0.0239} \exp\left[-0.223 \left\{\ln\left(\frac{g}{e}\right)\right\}^2\right] \exp\left[0.1153 \left\{\ln\left(\frac{\alpha}{60}\right)\right\}^2\right]$ $\exp\left[-0.2805 \left\{\ln\left(\frac{p}{e}\right)\right\}^2\right]$ $f = 3.1934 \times Re^{-0.3151} \left(\frac{e}{D}\right)^{0.268} \left(\frac{W}{w}\right)^{0.1132} \left(\frac{g}{e}\right)^{-0.1769} \left(\frac{Gd}{Lv}\right)^{0.0610}$ $\exp\left[0.0974 \left\{\ln\left(\frac{W}{w}\right)\right\}^2\right] \exp\left[-0.1065 \left\{\ln\left(\frac{Gd}{Lv}\right)\right\}^2\right] \exp\left[-0.6349 \left\{\ln\left(\frac{g}{e}\right)\right\}^2\right]$ $\left(\frac{\alpha}{60}\right)^{0.1553} \exp\left[-0.1527 \left\{\ln\left(\frac{\alpha}{60}\right)\right\}^2\right] \left(\frac{p}{e}\right)^{-0.7941} \exp\left[0.1486 \left\{\ln\left(\frac{p}{e}\right)\right\}^2\right]$

Kumar et. al. [53]	Discrete W-shaped ribs	Re = 3000-15000 p/e = 10 e/D <sub>h</sub> = 0.0168-0.0338 α = 30°-75°	<b>Nu = 2.16Nu<sub>s</sub></b> <b>f = 2.75f<sub>s</sub></b>	$Nu = 0.105 \times Re^{0.873} \left(\frac{e}{D_h}\right)^{0.453} \left(\frac{\alpha}{60}\right)^{-0.081} \exp\left[-0.59\left\{\ln\left(\frac{\alpha}{60}\right)\right\}^2\right]$ $f = 5.68 \times Re^{-0.40} \left(\frac{e}{D_h}\right)^{0.59} \left(\frac{\alpha}{60}\right)^{-0.081} \exp\left[-0.579\left\{\ln\left(\frac{\alpha}{60}\right)\right\}^2\right]$
Saini and Saini [54]	Arc shape ribs	Re = 2000-17000 p/e = 10 e/D = 0.0213-0.0422 α = 30°-75°	<b>Nu = 3.8Nu<sub>s</sub></b> <b>f = 1.75f<sub>s</sub></b>	$Nu = 0.001047 \times Re^{1.3186} \left(\frac{e}{D}\right)^{0.3772} \left(\frac{\alpha}{90}\right)^{-0.1198}$ $f = 0.14408 \times Re^{-0.17103} \left(\frac{e}{D}\right)^{0.1765} \left(\frac{\alpha}{90}\right)^{0.1185}$
Singh et. al. [56]	Multiple arc shape ribs	Re = 2200-22000 p/e = 4-16 e/D = 0.018-0.045 α = 30°-75° W/w = 1-7	<b>Nu = 5.07Nu<sub>s</sub></b> <b>f = 3.71f<sub>s</sub></b>	$Nu = 1.564 \times 10^{-4} \times Re^{1.343} \left(\frac{e}{D}\right)^{0.048} \left(\frac{W}{w}\right)^{0.407} \exp\left[-0.099\left\{\ln\left(\frac{W}{w}\right)\right\}^2\right]$ $\left(\frac{p}{e}\right)^{0.572} \exp\left[-0.148\left\{\ln\left(\frac{p}{e}\right)\right\}^2\right] \left(\frac{\alpha}{90}\right)^{-0.355} \exp\left[-0.272\left\{\ln\left(\frac{\alpha}{90}\right)\right\}^2\right]$ $f = 0.063 \times Re^{-0.16} \left(\frac{e}{D}\right)^{0.102} \left(\frac{W}{w}\right)^{0.277} \left(\frac{p}{e}\right)^{0.562}$ $\exp\left[-0.140\left\{\ln\left(\frac{p}{e}\right)\right\}^2\right] \left(\frac{\alpha}{90}\right)^{0.023} \exp\left[-0.013\left\{\ln\left(\frac{\alpha}{90}\right)\right\}^2\right]$
Pandey et. al. [58]	Multiple Arc shape ribs with gap	Re = 2100-21000 p/e = 4-16 e/D = 0.016-0.044 α = 30°-75° W/w = 1-7 d/x = 0.25-0.85 g/e = 0.5-2	<b>Nu = 5.85Nu<sub>s</sub></b> <b>f = 4.96f<sub>s</sub></b>	$Nu = 1.39 \times 10^{-4} \times Re^{1.3701} \left(\frac{d}{x}\right)^{-0.4997} \left(\frac{g}{e}\right)^{-0.0292} \left(\frac{W}{w}\right)^{0.4017}$ $\left(\frac{p}{e}\right)^{0.5854} \left(\frac{\alpha}{60}\right)^{-0.2235} \left(\frac{e}{D}\right)^{0.0931} \exp\left[-0.3989\left\{\ln\left(\frac{d}{x}\right)\right\}^2\right]$ $\exp\left[-0.2013\left\{\ln\left(\frac{g}{e}\right)\right\}^2\right] \exp\left[-0.129\left\{\ln\left(\frac{W}{w}\right)\right\}^2\right] \exp\left[-0.142\left\{\ln\left(\frac{p}{e}\right)\right\}^2\right]$ $\exp\left[0.5614\left\{\ln\left(\frac{\alpha}{60}\right)\right\}^2\right]$

				$f = 2.11 \times 10^{-1} \times Re^{-0.25} \left(\frac{d}{x}\right)^{-0.8888} \left(\frac{g}{e}\right)^{-0.079} \left(\frac{W}{w}\right)^{0.032}$ $\left(\frac{p}{e}\right)^{0.643} \left(\frac{\alpha}{60}\right)^{-2.546} \left(\frac{e}{D}\right)^{0.145} \exp\left[-0.662\left\{\ln\left(\frac{d}{x}\right)\right\}^2\right]$ $\exp\left[-0.496\left\{\ln\left(\frac{g}{e}\right)\right\}^2\right] \exp\left[-0.160\left\{\ln\left(\frac{p}{e}\right)\right\}^2\right] \exp\left[-3.96\left\{\ln\left(\frac{\alpha}{60}\right)\right\}^2\right]$
Saini and Verma [60]	Transverse dimple arrangement	Re = 2000-12000 e/D = 0.018-0.0379 p/e = 8-12		$Nu = 5.2 \times 10^{-4} \times Re^{1.27} \left(\frac{p}{e}\right)^{3.15} \exp\left[-2.12\left\{\log\left(\frac{p}{e}\right)\right\}^2\right] \left(\frac{e}{D}\right)^{0.033}$ $\exp\left[-1.3\left\{\log\left(\frac{e}{D}\right)\right\}^2\right]$ $f = 0.642 \times Re^{-0.423} (p/e)^{-0.465} \exp\left[0.054 \times \left\{\log\left(\frac{p}{e}\right)\right\}^2\right]$ $\left(\frac{e}{D}\right)^{-0.0214} \exp\left[0.84 \times \left\{\log\left(\frac{e}{D}\right)\right\}^2\right]$
Sethi et. al. [62]	Arc shape dimple arrangement	Re = 3600-18000 p/e = 10-20 e/D <sub>h</sub> = 0.021-0.036 $\alpha = 45^\circ - 75^\circ$	<b>THP = 1.18 – 1.88</b>	$Nu = 7.1 \times 10^{-3} \times Re^{1.1386} \left(\frac{e}{D_h}\right)^{0.3629} \left(\frac{p}{e}\right)^{-0.047} \left(\frac{\alpha}{60}\right)^{-0.0048}$ $\exp\left[-0.7792\left\{\ln\left(\frac{\alpha}{60}\right)\right\}^2\right]$ $f = 4.869 \times 10^{-1} \times Re^{-0.223} \left(\frac{e}{D_h}\right)^{0.2663} \left(\frac{p}{e}\right)^{-0.059} \left(\frac{\alpha}{60}\right)^{-0.0042}$ $\exp\left[-0.4801\left\{\ln\left(\frac{\alpha}{60}\right)\right\}^2\right]$

kumar et. al. [63]	Multiple V Dimple arrangement	$Re = 5000-17000$ $P_b/e_d = 8-11$ $e_d/d_d = 0.5-2$ $\alpha_a = 35^\circ-75^\circ$ $W_c/W_d = 1-6$ $e_d/D_h = 0.037$	<b><math>THP = 0.74 - 3.13</math></b>	$Nu = 9.35 \times 10^{-14} \times Re^{1.0655} \left(\frac{W_c}{W_d}\right)^{2.9832} \exp\left[-0.91 \left\{\ln\left(\frac{W_c}{W_d}\right)\right\}^2\right]$ $\left(\frac{p_b}{e_d}\right)^{2.99} \exp\left[\left\{\ln\left(\frac{p_b}{e_d}\right)\right\}^2\right] \left(\frac{e_d}{d_d}\right)^{-0.248} \exp\left[-0.1906 \left\{\ln\left(\frac{e_d}{d_d}\right)\right\}^2\right]$ $\left(\frac{\alpha_a}{55}\right)^{-1.096} \exp\left[-2.563 \left\{\ln\left(\frac{\alpha_a}{55}\right)\right\}^2\right]$ $f = 2.05 \times 10^{-5} \times Re^{-0.6307} \left(\frac{W_c}{W_d}\right)^{0.0853} \exp\left[0.0676 \left\{\ln\left(\frac{W_c}{W_d}\right)\right\}^2\right]$ $\left(\frac{p_b}{e_d}\right)^{19.13} \exp\left[\left\{\ln\left(\frac{p_b}{e_d}\right)\right\}^2\right] \left(\frac{e_d}{d_d}\right)^{-0.162} \exp\left[-0.341 \left\{\ln\left(\frac{e_d}{d_d}\right)\right\}^2\right]$ $\left(\frac{\alpha_a}{55}\right)^{-0.2254} \exp\left[-2.303 \left\{\ln\left(\frac{\alpha_a}{55}\right)\right\}^2\right]$
Bhushan and Singh [64]	Staggered protrusion ribs	$Re = 4000-20000$ $e/D = 0.03$ $d/D = 0.147-0.367$ $L/e = 25-37.5$	<b><math>Nu = 3.8Nu_s</math></b> <b><math>f = 2.2f_s</math></b>	$Nu = 2.1 \times 10^{-88} \times Re^{1.452} \left(\frac{S}{e}\right)^{12.94} \left(\frac{L}{e}\right)^{99.2} \left(\frac{d}{D}\right)^{-3.9}$ $\exp\left[-10.4 \left\{\log\left(\frac{S}{e}\right)\right\}^2\right] \exp\left[-77.2 \left\{\log\left(\frac{L}{e}\right)\right\}^2\right] \exp\left[-7.83 \left\{\log\left(\frac{d}{D}\right)\right\}^2\right]$ $f = 2.32 \times Re^{-0.201} \left(\frac{S}{e}\right)^{-0.383} \left(\frac{L}{e}\right)^{-0.484} \left(\frac{d}{D}\right)^{0.133}$

		S/e = 18.75-37.5		
Yadav et. al. [65]	Hemi-spherical protrusion arranged in arc shape	Re = 3600-18100 p/e = 12-24 e/D=0.015-0.03 $\alpha = 45^\circ-75^\circ$	$Nu = 2.89Nu_s$ $f = 2.93f_s$	$Nu = 0.154 \times Re^{1.017} \left(\frac{e}{D}\right)^{0.521} \left(\frac{p}{e}\right)^{-0.38} \left(\frac{\alpha}{60}\right)^{-0.213}$ $\exp\left[-2.023 \left\{\ln\left(\frac{\alpha}{60}\right)\right\}^2\right]$ $f = 7.207 \times Re^{-0.56} \left(\frac{e}{D}\right)^{0.176} \left(\frac{p}{e}\right)^{-0.18} \left(\frac{\alpha}{60}\right)^{0.038}$ $\exp\left[-1.412 \left\{\ln\left(\frac{\alpha}{60}\right)\right\}^2\right]$
Varun et al. [68]	Transverse and Inclined ribs combination	Re = 2000-14000 e/D <sub>h</sub> = 0.03 p/e = 3-8	Max thermal efficiency was at p/e=8	$Nu = 0.0006 \times Re^{1.213} \left(\frac{p}{e}\right)^{0.0104}$ $f = 1.0858 \times Re^{-0.3685} \left(\frac{p}{e}\right)^{0.0144}$
Patil et. al. [70-72]	Discrete V ribs combined with staggered ribs	Re = 3000-17000 e/D = 0.0433 p/e = 10 p'/p = 0.2-0.8 r/e = 1-2.5 s'/s = 0.2-0.8 $\alpha = 60^\circ$	$Nu = 3.18Nu_s$	$Nu = 0.0089 \times Re^{0.97} \exp\left[\frac{0.12}{1 + \{2.42 \ln\left(\frac{s'}{s}\right) + 1.19\}^2} + \frac{0.11}{1 + \{2.5 \ln\left(\frac{p'}{p}\right) + 1.41\}^2} + 0.14 \left[\ln\left(\frac{r}{e}\right)\right]^{0.71}\right]$ $f = 0.09 \times Re^{-0.18} \exp\left[\frac{0.10}{1 + \{3.18 \ln\left(\frac{s'}{s}\right) + 1.56\}^2} + \frac{0.08}{1 + \{2.6 \ln\left(\frac{p'}{p}\right) + 1.40\}^2} + 0.17 \left[\ln\left(\frac{r}{e}\right)\right]^{2.5}\right]$
Deo et. al [73]	multi-gap V down ribs combined with staggered ribs	Re = 4000-12000 p/e = 4-14 e/D <sub>h</sub> = 0.026-0.057 $\alpha = 40^\circ-80^\circ$	$Nu = 3.34Nu_s$ $f = 3.38f_s$	$Nu = 0.02253 \times Re^{0.98} \left(\frac{e}{D_h}\right)^{0.18} \left(\frac{p}{e}\right)^{-0.06} \left(\frac{\alpha}{60}\right)^{0.04}$ $f = 0.37156 \times Re^{-0.15} \left(\frac{e}{D_h}\right)^{0.65} \left(\frac{p}{e}\right)^{0.21} \left(\frac{\alpha}{60}\right)^{0.57}$

		w/e= 4.5 p/P = 0.65 g/e = 1 n = 2		
Gill et. al. [74]	Broken arc ribs combined with staggered ribs	Re = 2000-18000 e/D <sub>h</sub> =0.0433 p/e = 10 p'/p= 0.4 r/g = 1-6 w'/w = 0.65 g/e = 1 α/90 = 0.333	<b>Nu = 3.06Nu<sub>s</sub></b> <b>f = 2.5f<sub>s</sub></b>	-----
Saini and Saini [75]	Expanded Metal Mesh	Re = 1900-13000 e/D = 0.012-0.039 L/e = 25-71.87 S/e = 15.62-46.87	<b>Nu = 4Nu<sub>s</sub></b> <b>f = 5f<sub>s</sub></b>	$Nu = 4 \times 10^{-4} \times \left( Re \right)^{1.22} \left( \frac{e}{D} \right)^{0.625} \left( \frac{S}{10e} \right)^{2.22} \left( \frac{L}{10E} \right)^{2.66}$ $\exp \left[ \left\{ -1.25 \left( \ln \left( \frac{S}{10e} \right) \right)^2 \right\} \right] \exp \left[ \left\{ -0.824 \left( \ln \left( \frac{L}{10e} \right) \right)^2 \right\} \right]$ $f = 0.815 \times \left( Re \right)^{-0.361} \left( \frac{L}{e} \right)^{0.266} \left( \frac{S}{10e} \right)^{-0.19} \left( \frac{10e}{D} \right)^{0.591}$
Karmare and Tikekar [77]	Metal grit ribs	Re = 4000-17000 e/D <sub>h</sub> = 0.035-0.044 p/e = 12.5-36 l/s = 1-1.72	<b>Nu = 1.86Nu<sub>s</sub></b> <b>f = 2.13f<sub>s</sub></b>	$Nu = 2.4 \times 10^{-3} \times Re^{1.3} \left( \frac{e}{D_h} \right)^{0.42} \left( \frac{l}{s} \right)^{-0.146} \left( \frac{p}{e} \right)^{-0.27}$ $f = 15.55 \times Re^{-0.263} \left( \frac{e}{D_h} \right)^{0.91} \left( \frac{l}{s} \right)^{-0.27} \left( \frac{p}{e} \right)^{-0.51}$
Karwa et. al. [79]	Chamfered rib shape	Re = 3000-20000 e/D <sub>h</sub> =0.0141-0.0328 p/e = 4.5-8.5 W/H = 4.8-12	<b>f = (1.8 – 3.9)f<sub>s</sub></b>	$g = 103.77 \times e^{-0.006\phi} \left( \frac{W}{H} \right)^{0.5} \left( \frac{p}{e} \right)^{-2.56} \exp[0.7343] \left\{ \ln \left( \frac{p}{e} \right)^2 \right\} (e^+)^{-0.31}$ <p>For 7 ≤ e<sup>+</sup> &lt; 20</p> $g = 32.26 \times \left( \frac{W}{H} \right)^{0.5} \left( \frac{p}{e} \right)^{-2.56} \exp[0.7343] \left\{ \ln \left( \frac{p}{e} \right)^2 \right\} (e^+)^{-0.08}$ <p>For 20 ≤ e<sup>+</sup> &lt; 60</p>

		$\phi = -15^\circ - 18^\circ$ $e^+ = 5-60$		$R = 1.66 \times e^{-0.0078\phi} \left(\frac{W}{H}\right)^{-0.4} \left(\frac{p}{e}\right)^{2.695} \exp\left[-0.762 \left\{\ln\left(\frac{p}{e}\right)\right\}^2\right]$ <p>For <math>5 \leq e^+ &lt; 20</math></p> $R = 1.325 \times e^{-0.0078\phi} \left(\frac{W}{H}\right)^{-0.4} \left(\frac{p}{e}\right)^{2.695} \exp\left[-0.762 \left\{\ln\left(\frac{p}{e}\right)\right\}^2\right]$ <p>For <math>20 \leq e^+ &lt; 60</math></p>
Bhagoria et al.[81]	Wedge shaped rib	$Re = 3000-18000$ $e/D_h = 0.015-0.033$ $60.17\phi^{-1.0264} < p/e < 12.12$ $\phi = 8^\circ - 15^\circ$	$Nu = 2.4Nu_s$ $f = 5.3f_s$	$Nu = 1.89 \times 10^{-4} \times Re^{1.21} \left(\frac{e}{D_h}\right)^{0.462} \left(\frac{p}{e}\right)^{2.94} \exp\left[-0.71 \left\{\ln\left(\frac{p}{e}\right)\right\}^2\right]$ $\left(\frac{\phi}{10}\right)^{-0.018} \exp\left[-1.5 \left\{\ln\left(\frac{\phi}{10}\right)\right\}^2\right]$ $f = 12.44 \times Re^{-0.18} \left(\frac{e}{D_h}\right)^{0.99} \left(\frac{p}{e}\right)^{-0.52} \left(\frac{\phi}{10}\right)^{0.49}$
Jaurker et. al. [82]	rib-grooved artificial coarseness	$Re = 3000-21000$ $e/D=0.0181-0.0363$ $p/e = 4.5-10$ $g/p = 0.3-0.7$	$Nu = 2.7Nu_s$ $f = 3.6f_s$	$Nu = 0.002062 \times Re^{0.936} \left(\frac{e}{D}\right)^{0.349} \left(\frac{p}{e}\right)^{3.318} \exp\left[-0.868 \left\{\ln\left(\frac{p}{e}\right)\right\}^2\right]$ $\left(\frac{g}{p}\right)^{1.108} \exp\left[2.486 \left\{\ln\left(\frac{g}{p}\right)\right\}^2 + 1.406 \left\{\ln\left(\frac{g}{p}\right)\right\}^3\right]$ $f = 0.001227 \times Re^{-0.199} \left(\frac{e}{D}\right)^{0.585} \left(\frac{p}{e}\right)^{7.19} \exp\left[-1.854 \left\{\ln\left(\frac{p}{e}\right)\right\}^2\right]$ $\left(\frac{g}{p}\right)^{0.645} \exp\left[1.513 \left\{\ln\left(\frac{g}{p}\right)\right\}^2 + 0.8662 \left\{\ln\left(\frac{g}{p}\right)\right\}^3\right]$
Layek et. al. [83]	repeated integral transverse chamfered rib groove coarseness	$Re = 3000-21000$ $e/D_h=0.022-0.04$ $P/e = 4.5-10$ $g/P = 0.3-0.6$ $\phi = 5^\circ - 30^\circ$	$Nu = 3.24Nu_s$ $f = 3.78f_s$	$Nu = 0.00225 \times \left(Re\right)^{0.92} \left(\frac{e}{D_h}\right)^{0.52} \left(\frac{P}{e}\right)^{1.72} \exp\left[-0.22(\ln \phi)^2\right]$ $\exp\left[-0.46 \left\{\ln\left(\frac{P}{e}\right)\right\}^2\right] \left(\frac{g}{P}\right)^{-1.21} \phi^{1.24} \exp\left[-0.74 \left\{\ln\left(\frac{g}{P}\right)\right\}^2\right]$ $f = 0.00245 \times \left(Re\right)^{-0.124} \left(\frac{e}{D_h}\right)^{0.346} \left(\frac{P}{e}\right)^{4.32} \exp\left[-0.005\phi\right]$ $\exp\left[-1.09 \left\{\ln\left(\frac{P}{e}\right)\right\}^2\right] \left(\frac{g}{P}\right)^{-1.124} \exp\left[-0.68 \left\{\ln\left(\frac{g}{P}\right)\right\}^2\right]$